JEM Journal of Experimental Medicine

ARTICLE

A human STAT3 gain-of-function variant drives local Th17 dysregulation and skin inflammation in mice

Kelsey A. Toth[1], Erica G. Schmitt[1], Ana Kolicheski[1], Zev J. Greenberg[2], Elizabeth Levendosky[3], Nermina Saucier[1], Kelsey Trammel[1], Vasileios Oikonomou[4], Michail S. Lionakis[4], Eynav Klechevsky[5], Brian S. Kim[6,7], Laura G. Schuettpelz[2], Naresha Saligrama[3,5,8], and Megan A. Cooper[1,5]

Germline gain-of-function (GOF) variants in *STAT3* cause an inborn error of immunity associated with early-onset polyautoimmunity and immune dysregulation. To study tissue-specific immune dysregulation, we used a mouse model carrying a missense variant (p.G421R) that causes human disease. We observed spontaneous and imiquimod (IMQ)-induced skin inflammation associated with cell-intrinsic local Th17 responses in STAT3 GOF mice. CD4⁺ T cells were sufficient to drive skin inflammation and showed increased *Il22* expression in expanded clones. Certain aspects of disease, including increased epidermal thickness, also required the presence of STAT3 GOF in epithelial cells. Treatment with a JAK inhibitor improved skin disease without affecting local Th17 recruitment and cytokine production. These findings collectively support the involvement of Th17 responses in the development of organ-specific immune dysregulation in STAT3 GOF and suggest that the presence of STAT3 GOF in tissues is important for disease and can be targeted with JAK inhibition.

Introduction

Signal transducer and activator of transcription 3 (STAT3) is a transcription factor involved in cell proliferation, differentiation, and the induction and regulation of immune responses (Levy and Lee, 2002; O'Shea et al., 2002; Yu et al., 2009). Germline heterozygous gain-of-function (GOF) variants in *STAT3* lead to an inborn error of immunity (IEI) characterized by immune dysregulation and early-onset multiorgan autoimmunity (Flanagan et al., 2014; Haapaniemi et al., 2015; Milner et al., 2015; Toth et al., 2023; Vogel et al., 2023). Patients with STAT3 GOF syndrome present with variable clinical manifestations. Common features include lymphoproliferation, autoimmune cytopenias, enteropathy, endocrinopathies, skin disease, interstitial lung disease, and growth defects (Leiding et al., 2023). The majority of germline *STAT3* GOF variants lead to increased transcriptional activity of *STAT3*, but unlike somatic variants associated with cancer, do not result in autophosphorylation (Vogel et al., 2023). Thus, therapeutics that block upstream activation of STAT3 signaling, including JAK inhibitors (JAKinibs) and IL-6 receptor antagonists, are used to treat patients (Forbes et al., 2018; Silva-Carmona et al., 2020; Vogel et al., 2023).

STAT3 is activated in multiple cell types by many different cytokines associated with pro- and anti-inflammatory responses, including IL-6, IL-10, IL-21, IL-23, and type I interferons (IFNs) (Gaffen et al., 2014; Levy and Lee, 2002; O'Shea and Plenge, 2012; O'Shea et al., 2015). In T cells, STAT3 is important in the polarization and function of T-helper 17 cells (Th17), which maintain homeostasis with commensal organisms and eliminate specific pathogens at mucosal and barrier interfaces. IL-6, IL-23, and IL-21 signal through STAT3 in Th17 cells to induce expression of RORγt and RORα, IL-17A, IL-22, and IL-23R (Hillmer et al., 2016; Kane et al., 2014; Vogel et al., 2015). Conversely, STAT3 suppresses regulatory T cell (Treg) development by binding *FOXP3* (Kane et al., 2014). However, analysis of peripheral blood from patients has shown that less than one-third of evaluated STAT3 GOF patients have elevated Th17 cells, and less than half had low Treg frequencies compared to healthy donors (Leiding et al., 2023). Recent studies from our group and

[1]Department of Pediatrics, Division of Rheumatology, Washington University School of Medicine, St. Louis, MO, USA; [2]Department of Pediatrics, Division of Hematology and Oncology, Washington University School of Medicine, St. Louis, MO, USA; [3]Department of Neurology, Washington University School of Medicine, St. Louis, MO, USA; [4]Fungal Pathogenesis Section, Laboratory of Clinical Immunology and Microbiology, National Institute of Allergy and Infectious Diseases, Bethesda, MD, USA; [5]Department of Pathology and Immunology, Division of Immunobiology, Washington University School of Medicine, St. Louis, MO, USA; [6]Kimberly and Eric J. Waldman Department of Dermatology, Icahn School of Medicine at Mount Sinai, Precision Immunology Institute, Friedman Brain Institute, Mark Lebwohl Center for Neuroinflammation and Sensation, New York, NY, USA; [7]Allen Discovery Center for Neuroimmune Interactions, New York, NY, USA; [8]Bursky Center for Human Immunology & Immunotherapy, Washington University School of Medicine, St. Louis, MO, USA.

Correspondence to Megan A. Cooper: cooper_m@wustl.edu.

others have suggested that peripheral blood Tregs from STAT3 GOF patients are similar to healthy controls, while effector CD8⁺ T cells are expanded in some patients (Masle-Farquhar et al., 2022; Schmitt et al., 2022). Understanding the cause of T cell dysregulation and how, if at all, this drives disease in STAT3 GOF patients remains challenging due to the pleiotropic nature of *STAT3*, prior immunosuppressive therapy, and tissue sampling limited to peripheral blood.

Previous studies of STAT3 GOF mouse models from our group and others have shown that STAT3 GOF causes T cell dysregulation and lymphoproliferation, similar to patients (Masle-Farquhar et al., 2022; Schmitt et al., 2022; Warshauer et al., 2021; Woods et al., 2022). We previously demonstrated an expansion of effector CD4⁺ and CD8⁺ T cells in older STAT3 GOF mice and Th1 skewing in a colitis model (Schmitt et al., 2022). Surprisingly, this was not associated with overt Treg dysfunction, but with impaired peripheral Treg (pTreg) differentiation (Schmitt et al., 2022). Two other studies highlighted CD8⁺ T cell dysregulation with STAT3 GOF that drives accelerated autoimmune diabetes on the non-obese diabetic (NOD) background or lymphoproliferation in aged mice (Masle-Farquhar et al., 2022; Warshauer et al., 2021).

Patients with STAT3 GOF generally present after 2 years of age, and combined with the heterogeneity of disease, even among related individuals with the same variant, suggests that environmental factors, including common infections and inflammatory triggers, influence disease phenotype (Leiding et al., 2023). We identified spontaneous skin disease in a murine model of heterozygous STAT3 GOF (*Stat3*$^{p.G421R/+}$) (Schmitt et al., 2022), referred to as "STAT3 GOF" here) associated with a local, but not systemic, Th17 response. We hypothesized that T cell dysregulation in STAT3 GOF patients is triggered by an inflammatory stimulus and modeled this in younger mice by topical administration of the TLR7 agonist imiquimod (IMQ). This resulted in similar disease and increased local Th17 responses. Skin inflammation is not dependent on CD8⁺ or γδ T cells, and STAT3 GOF CD4⁺ T cells are sufficient to drive skin inflammation and exhibit cell-intrinsic Th17 skewing and clonal expansion. Disease is enhanced when STAT3 GOF is also present in skin epithelial cells, which responded to JAK inhibition. These data suggest the mechanisms driving development of autoimmunity are organ-specific in STAT3 GOF syndrome.

Results

Older adult STAT3 GOF (p.G421R) mice develop spontaneous skin inflammation

We recently generated a murine model of STAT3 GOF syndrome in which the p.G421R variant was introduced into C57BL/6 mice by CRISPR/Cas9 (Schmitt et al., 2022). In patients and mice, the p.G421R variant in the DNA binding domain does not confer constitutive STAT3 activation, but rather delayed STAT3 dephosphorylation following stimulation (Milner et al., 2015; Schmitt et al., 2022). Young STAT3 GOF mice exhibit splenomegaly and lymphadenopathy, with an expansion of effector T cells by early adulthood that persists as mice age (Schmitt et al., 2022).

While young adult (7–9 wk old) STAT3 GOF mice do not have organ-specific disease beyond lymphoproliferation, older adult (>18 wk old) STAT3 GOF mice had spontaneous ear swelling compared with wild-type (WT) littermates (Fig. 1, A and B). Dermatitis was significant by 18 wk and increased with age (Fig. 1 B). Patients with STAT3 GOF have a high frequency of skin disease (~60%), and both psoriasiform dermatitis and scleroderma have been observed in patients with the p.G421R variant (Khoury et al., 2017; Leiding et al., 2023; Milner et al., 2015). Thus, this phenotype is relevant to clinical disease. Histopathologic analysis of ear sections revealed increased epidermal thickness, cellular infiltrate, and pathologic score in aged STAT3 GOF mice compared with WT littermates (Fig. 1, C and D).

Analysis of skin immune cells revealed neutrophil and monocyte infiltration, with significantly increased CD4⁺ and CD8⁺ T cell frequency and number (Fig. 1 E and Fig. S1 A). We previously observed increased CD4⁺ IFNγ⁺ cells in the spleen of STAT3 GOF mice by 20 wk of age (Schmitt et al., 2022), but not in the skin (data not shown), suggesting tissue-specific differences in immune responses. Instead, the skin of older STAT3 GOF mice had increased frequencies and numbers of CD4⁺ T cells expressing IL-17A, IL-22, and the Th17 lineage-defining transcription factor RORγt, as well as IL-17A⁺ IL-22⁺ double-positive CD4⁺ T cells (Fig. 1 F and Fig. S1 B). Within the γδ T cell population, which are major producers of IL-17A and IL-22 in mouse skin (Cai et al., 2011; Sumaria et al., 2011), there was an increase in both frequency and number of total IL-22⁺ and IL-17A⁺ IL-22⁺ double-positive cells, but not total IL-17A⁺ or RORγt⁺ γδ T cells in older mice (Fig. 1 G and Fig. S1 B), indicating STAT3 GOF also influences IL-22 production in skin-resident T cells.

As we previously observed (Schmitt et al., 2022), older adult mice had lymphoproliferation with increased cellularity of cervical lymph nodes (CLN) and spleen (data not shown). There was no significant difference in the frequency of IL-17A⁺ CD4⁺ T cells in the CLN or spleen (Fig. 1, H and I), with variably increased numbers in these organs, consistent with increased cellularity (Fig. S1, C and D). However, the frequency and number of total IL-22⁺ CD4⁺ T cells were increased in the CLN and spleen (Fig. 1, H and I; and Fig. S1, C and D). The frequency of IL-17A⁺ IL-22⁺ double-positive CD4⁺ T cells was only increased in the spleen, but total numbers of this population were increased in both the CLN and spleen (Fig. 1, H and I; and Fig. S1, C and D). Total numbers of IL-17A⁺, IL-22⁺, and IL-17A⁺ IL-22⁺ double-positive γδ T cells were also increased in the CLN, but not the spleen (Fig. S1, E and F). This suggests that the Th17 phenotype is tissue-specific, potentially with increased peripheral IL-22 expression due to STAT3 GOF.

Having observed increased Th17 in older adult mice in vivo, we tested in vitro Th17 polarization in young adult STAT3 GOF mice. STAT3 GOF naïve or bulk CD4⁺ T cells cultured under Th17-polarizing conditions in vitro showed increased Th17 polarization with low levels of IL-6 compared with WT (Fig. 2, A and B), similar to in vitro Th17 skewing reported in the NOD model (Warshauer et al., 2021). Interestingly, bulk splenic CD4⁺ T cells cultured without IL-6 produced significant IL-17 (Fig. 2 B), suggesting that TCR ligation and TGFβ signaling are sufficient to induce Th17 polarization in peripheral STAT3 GOF CD4⁺ T cells.

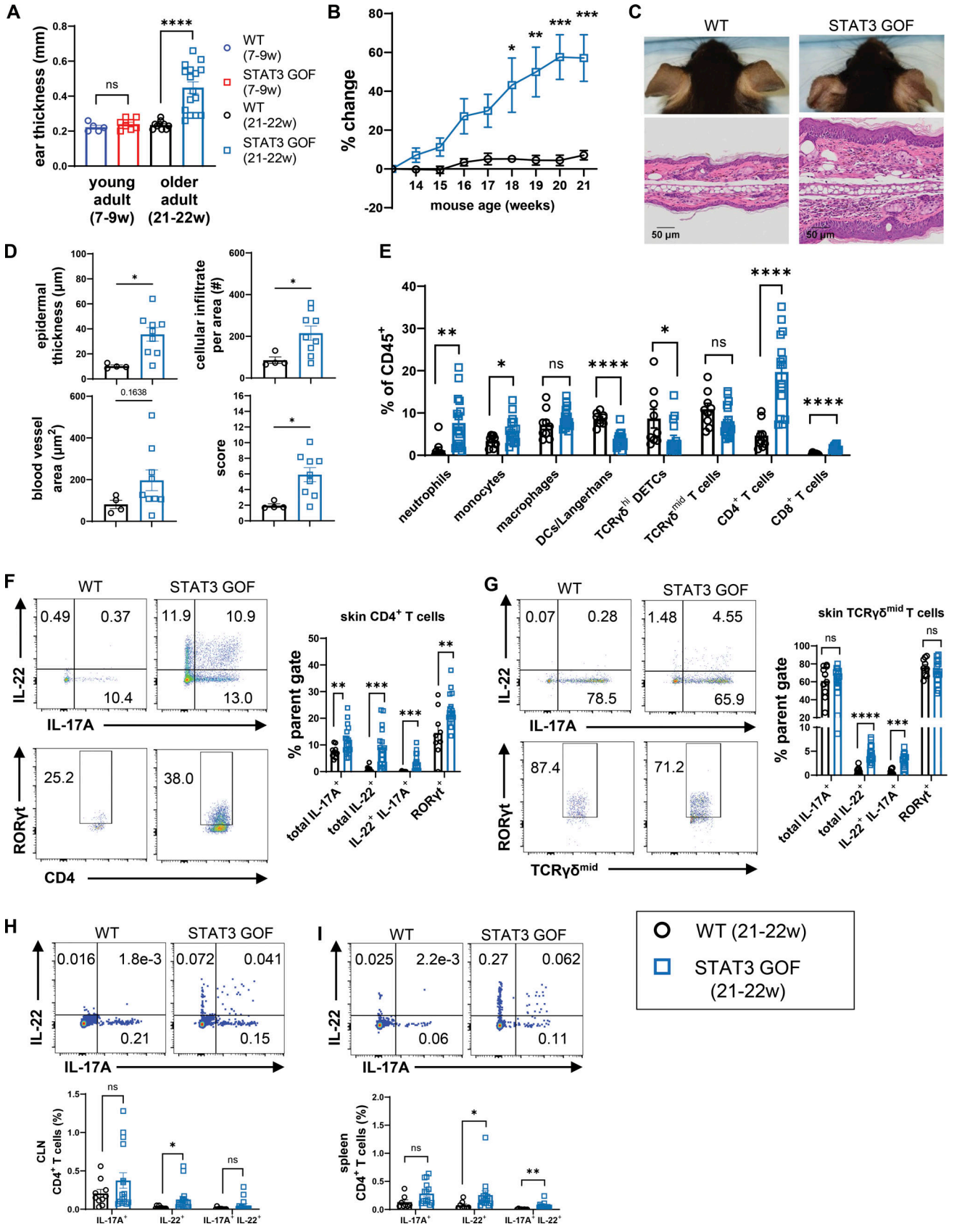

Figure 1. **Older adult STAT3 GOF (p.G421R) mice develop spontaneous skin inflammation. (A)** Ear thickness of young adult and older adult mice. w, week. **(B)** Percent change in ear thickness of older adult mice relative to baseline at 13 wk. **(C)** Representative pictures of older adult mice and H&E ear sections. **(D)** Histological measurements of ears. **(E)** Quantification of skin immune cell frequencies by flow cytometry, including dendritic epidermal T cells

(DETCs). **(F and G)** (F) Representative flow plots and quantification of IL-17A$^+$, RORγt$^+$, and IL-22$^+$ skin CD4$^+$ and (G) skin γδ T cells. Cytokines were assessed after PMA/ionomycin stimulation. **(H and I)** (H) Representative flow plot and quantification of IL-17A$^+$ and IL-22$^+$ CD4$^+$ T cells in CLN and (I) spleen T cells after PMA/ionomycin stimulation. Bars: mean ± SEM. Statistical significance determined by unpaired two-tailed or Welch's *t* test (A and D–I), or two-way repeated measures ANOVA with Šídák's multiple comparisons test (B), *P < 0.05, **P < 0.01, ***P < 0.001, ****P < 0.0001. Data are representative of >3 experiments with 4–16 mice/group.

Collectively, these findings demonstrate that STAT3 GOF enhances Th17 differentiation in vivo and in vitro and is associated with spontaneous skin disease with local infiltration of Th17 cells.

Topical IMQ elicits severe skin inflammation and a Th17 response in young adult STAT3 GOF mice

We hypothesize that organ-specific disease due to STAT3 GOF is partly dictated by environmental factors that initiate inflammation. To test this hypothesis, we used the IMQ model of psoriasiform dermatitis (van der Fits et al., 2009) to determine if an in vivo inflammatory challenge in younger mice would lead to inflammation similar to spontaneous skin disease in older adult STAT3 GOF mice in specific pathogen–free housing.

IMQ is a TLR7 ligand that causes skin inflammation via induction of STAT3-activating cytokines such as type I IFN, IL-6, IL-22, and IL-23 (Suzuki et al., 2000; Van Belle et al., 2012; van der Fits et al., 2009; Wohn et al., 2013). IL-6 and IL-23 induce IL-17 and IL-22 production by Th17 and γδ T cells, which in turn mediate neutrophil recruitment and stimulate keratinocyte proliferation resulting in hyperplasia (Flutter and Nestle, 2013). By day 5 of topical IMQ treatment, ear swelling was substantially greater in young adult STAT3 GOF mice compared with WT littermates, with visible redness and scaling of the skin (Fig. 3, A and B). IMQ-treated STAT3 GOF mice also had more severe disease with significantly increased epidermal thickness and cellular infiltrate (Fig. 3 C). Another model of heterozygous STAT3 GOF (*Stat3*$^{p.T716M/+}$, transactivation domain variant) generated in our laboratory also had increased ear swelling compared with WT littermates following IMQ treatment (Fig. 3 D). This is consistent with a recent report of spontaneous skin inflammation of unknown etiology in homozygous *Stat3*$^{p.T716M/T716M}$ mice from another group (Masle-Farquhar et al., 2022), and demonstrates the penetrance of the skin phenotype with different STAT3 GOF variants.

Total cellularity of the skin was not changed in IMQ-treated STAT3 GOF (*Stat3*$^{p.G421R/+}$) mice (Fig. S2 A); however, there was a significant influx of skin-infiltrating neutrophils and

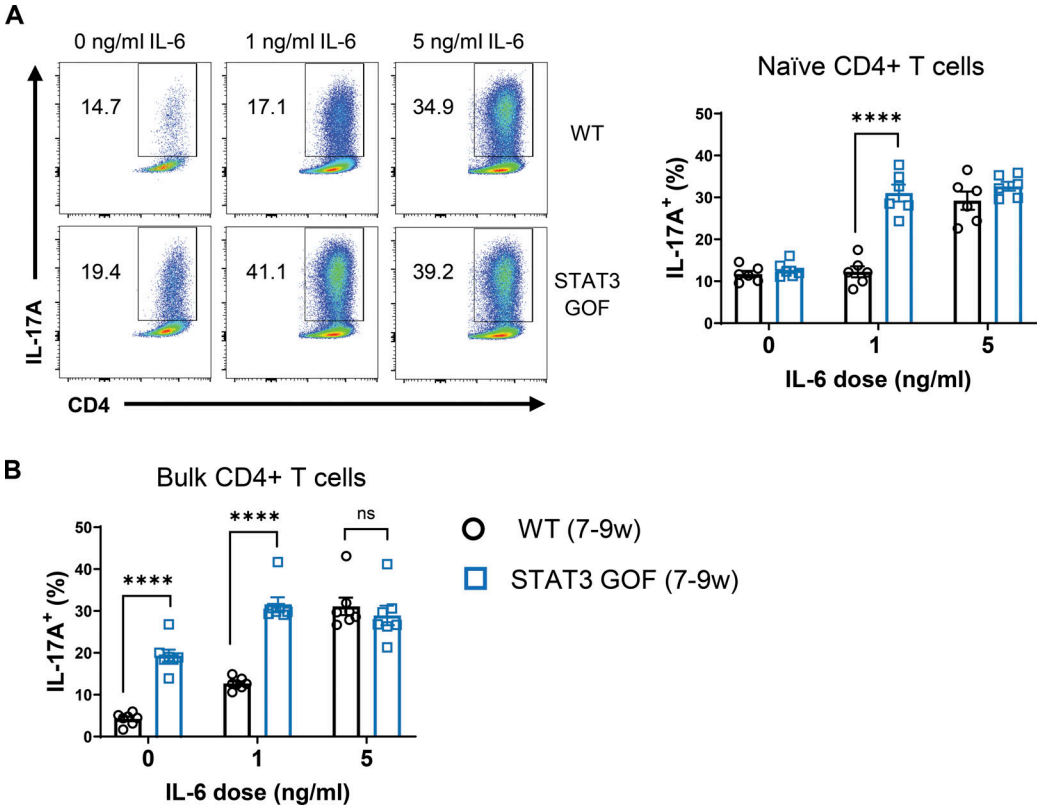

Figure 2. **Th17 polarization is enhanced in naïve and bulk STAT3 GOF CD4$^+$ T cells. (A)** Representative flow plot and quantification of IL-17A following Th17 polarization of naïve CD4$^+$ T cells with varying concentrations of IL-6. **(B)** Quantification of Th17 polarization of bulk splenic CD4$^+$ T cells with varying concentrations of IL-6. w, week. Bars: mean ± SEM. Statistical significance was determined by two-way ANOVA with Sidak's multiple comparisons test (A and B), ****P < 0.0001. Data represent two independent experiments with six to seven mice/group.

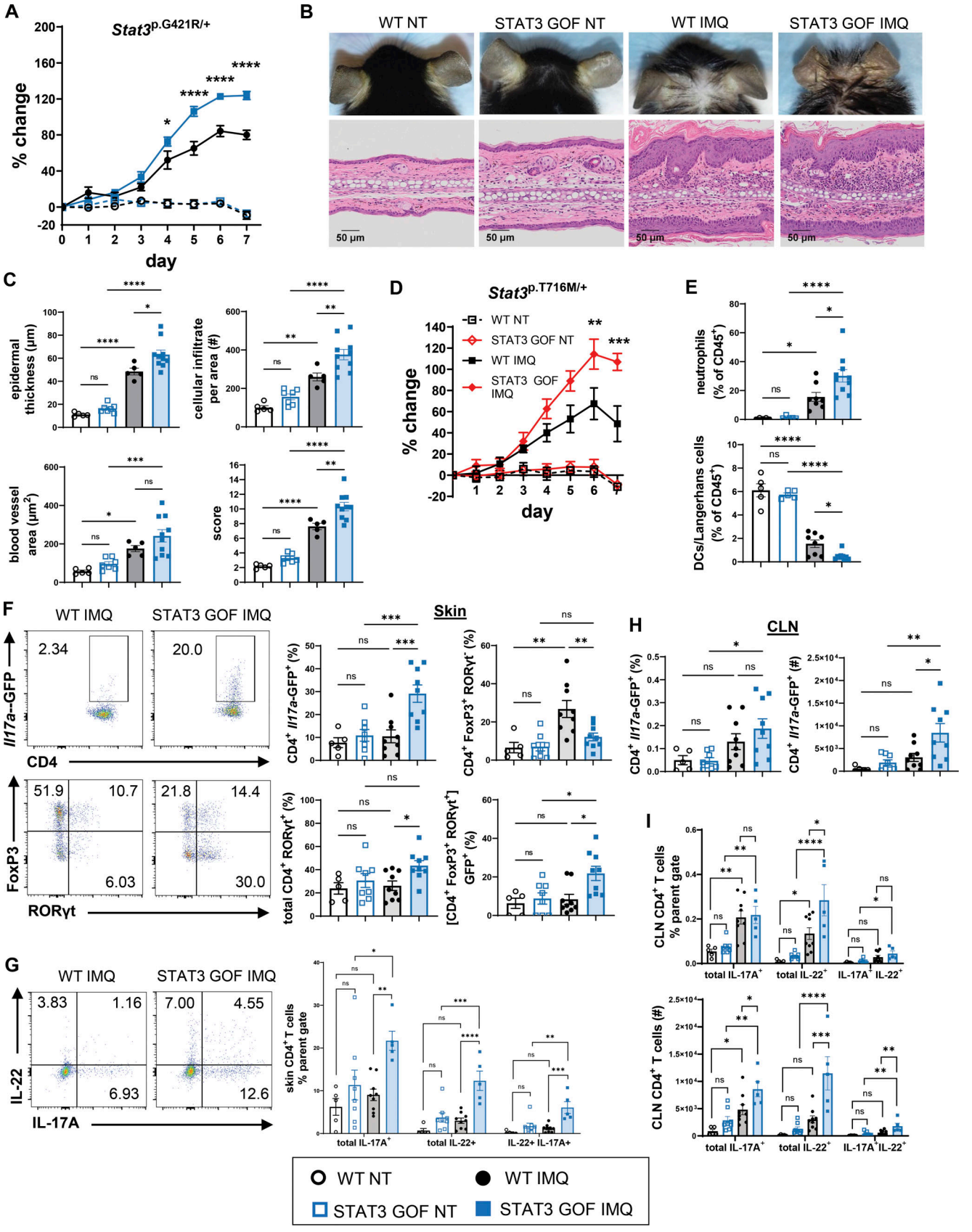

Figure 3. **Topical IMQ elicits severe skin inflammation and a Th17 response in young adult STAT3 GOF mice. (A)** Adult WT and *Stat3*$^{p.G421R/+}$ littermates were treated with topical 5% IMQ cream on both ears for 7 consecutive days. Percent change in ear thickness of IMQ-treated young adult mice relative to baseline. **(B)** Representative pictures of NT and IMQ-treated mice and H&E ear sections. **(C)** Histological measurements of ears. **(D)** IMQ-treated adult WT and

Stat3$^{p.T716M/+}$ littermates. Percent change in ear thickness during the course of IMQ treatment relative to baseline. **(E)** Frequency and quantification of skin immune cells of STAT3 GOF (p.G421R) mice. **(F)** Analysis of immune cell populations from the skin of IMQ-treated adult *Il17a*-GFP and STAT3 GOF x *Il17a*-GFP littermates, with representative flow plots gated on CD4$^+$ T cells. Quantification of skin CD4$^+$ T cells that are *Il17a*-GFP$^+$, RORγt$^+$, or FoxP3$^+$ RORγt$^-$. Lower right represents quantification of the percent of CD4$^+$FoxP3$^+$ RORγt$^+$ (parent gate) that are *Il17a*-GFP$^+$. **(G)** Representative flow plot and quantification of skin IL-17A$^+$ and IL-22$^+$ CD4$^+$ T cells after PMA/ionomycin. **(H)** Frequency and total number of CLN *Il17a*-GFP$^+$ CD4$^+$ T cells. **(I)** Frequency and total number of CLN IL-17A$^+$ and IL-22$^+$ CD4$^+$ T cells after PMA/ionomycin. **(E–I)** IL-17 GFP mice treated with IMQ. Bars: mean ± SEM. Statistical significance determined by two-way repeated measures ANOVA with Šídák's multiple comparisons test (A and D) or one-way ANOVA with Šídák's multiple comparisons test (C and E–I). *P < 0.05, **P < 0.01, ***P < 0.001, ****P < 0.0001. Data represent three to four experiments with 5–12 mice/group.

decreased dendritic cell (DC)/Langerhans cells compared with WT (Fig. 3 E). CLN total cell number was increased in IMQ-treated STAT3 GOF mice, but not WT (Fig. S2 B), which had frequencies and numbers of total T and B cells similar to untreated STAT3 GOF mice (Fig. S2 C).

STAT3 GOF mice were crossed with an IL-17 GFP reporter strain to track local Th17 cells following IMQ. The frequency of skin *Il17a*-GFP$^+$ and total RORγt$^+$ CD4$^+$ T cells of STAT3 GOF mice was the same as WT at baseline, corresponding with a lack of spontaneous skin disease in young adults (Fig. 3 F). Additionally, there was no difference in the frequency of *Il17a*-GFP$^+$ CD4$^+$ T cells in the peripheral blood at baseline (data not shown). Following IMQ, there was a large increase in *Il17a*-GFP$^+$ and RORγt$^+$ CD4$^+$ T cells of the skin only in STAT3 GOF mice (Fig. 3 F). Interestingly, Treg frequency (CD4$^+$Foxp3$^+$ RORγt$^-$) increased in IMQ-treated WT, but not STAT3 GOF mice (Fig. 3 F), suggesting impaired differentiation and/or recruitment of pTregs, similar to the T cell transfer model (Schmitt et al., 2022). While the frequency of FoxP3$^+$ RORγt$^+$ double-positive CD4$^+$ T cells was increased in the skin of both WT and STAT3 GOF IMQ-treated mice (data not shown), these cells produced increased IL-17 in STAT3 GOF mice based on *Il17*-GFP expression (Fig. 3 F). This finding suggests that the local inflammatory environment may lead to alterations in the Treg phenotype in STAT3 GOF mice.

The frequencies of total IL-17A$^+$, total IL-22$^+$, and IL-17A$^+$ IL-22$^+$ double-positive skin CD4$^+$ T cells from STAT3 GOF mice were also increased following ex vivo PMA and ionomycin stimulation (Fig. 3 G). Together, these data demonstrate a strong local Th17 response in STAT3 GOF in response to IMQ that is not observed in WT mice. Consistent with prior studies, skin γδ T cells produced IL-17A and IL-22 after IMQ treatment (Fig. S2, D and E) (Cai et al., 2011). In the skin, STAT3 GOF mice had a higher frequency of total IL-22$^+$ and IL-17A$^+$ IL-22$^+$ double-positive γδ T cells compared with WT, with a similar frequency of total IL-17A$^+$ cells following PMA and ionomycin stimulation (Fig. S2 E).

In the CLN, *Il17*-GFP$^+$ CD4$^+$ T cells were increased in both frequency and number in IMQ-treated STAT3 GOF, but not WT mice (Fig. 3 H). The frequency and number of total IL-22$^+$ CD4$^+$ T cells in the CLN were increased in IMQ-treated STAT3 GOF compared with WT (Fig. 3 I). Frequencies and numbers of *Il17*-GFP$^+$ RORγt$^+$ γδ T cells in the CLN were increased in both WT and STAT3 GOF after IMQ (Fig. S2 F). Additionally, there was a significant increase in the number of total IL-22$^+$ and IL-17A$^+$ IL-22$^+$ double-positive STAT3 GOF γδ T cells compared with WT after IMQ (Fig. S2 G). Together, these data suggest STAT3 GOF increases IL-22 expression in CD4$^+$ and γδ T cells of the draining lymph nodes following IMQ. Frequencies of Tregs, Foxp3$^+$ RORγt$^+$, and total RORγt$^+$ CD4$^+$ T cells were similar between STAT3 GOF and WT with IMQ in the CLN, with increased total cell numbers of these populations associated with the increased cellularity of STAT3 GOF CLNs (Fig. S2 H).

In summary, IMQ treatment elicited disease and local inflammatory responses in STAT3 GOF mice, with ear swelling and neutrophil infiltration, increased cellularity of the draining lymph nodes, and increased Th17 and IL-22–producing γδ T cells in the skin. Together, these data support a role for local inflammation mediated by Th17 cells and IL-22 in STAT3 GOF mice, and that a STAT3-activating stimulus, such as IMQ, can trigger local inflammation leading to disease.

CD4$^+$ T cells are sufficient, and γδ T cells and CD8$^+$ T cells are not required to mediate IMQ-induced inflammation in STAT3 GOF mice

To test if adaptive immune cells were required for skin inflammation, STAT3 GOF mice were crossed to *Rag-1*$^{-/-}$ mice and treated with IMQ. *Rag1*-deficient mice had milder ear swelling, and there was no difference in ear thickness between *Rag1*$^{-/-}$ WT and *Rag1*$^{-/-}$ STAT3 GOF mice (Fig. 4 A). Similarly, there were no differences in overall pathological score or individual histological measurements (Fig. 4, B and C). These data indicate that adaptive immune cells are required for IMQ-induced ear swelling and skin pathology due to STAT3 GOF. To test if γδ T cells were required to drive disease, STAT3 GOF mice were crossed to mice lacking the *Tcrd* gene (*Tcrd*$^{-/-}$ mice) and treated with IMQ. In the absence of γδ T cells, increased disease in STAT3 GOF mice persisted, including ear swelling (Fig. 4 D), neutrophil recruitment (Fig. S3 A), and measures of skin pathology (data not shown). Thus, γδ T cells are not required for IMQ-induced skin disease due to STAT3 GOF. Recent reports from mouse models of other STAT3 GOF variants have described dysregulated CD8$^+$ T cells in type I diabetes (Warshauer et al., 2021) and spontaneous skin pathology (Masle-Farquhar et al., 2022). To test if CD8$^+$ T cells were required, *Tcrd*$^{-/-}$ mice were depleted of CD8$^+$ cells prior to and during IMQ treatment. Again, there was increased ear swelling with STAT3 GOF in the absence of both γδ T and CD8$^+$ T cells (Fig. 4 E). Overall pathologic score was increased in CD8-depleted STAT3 GOF, driven mostly by increased epidermal thickness (Fig. S3 B). Although neutrophil numbers in the skin were not significantly different (Fig. S3 C), the frequency of IL-17A$^+$ and IL-22$^+$ CD4$^+$ T cells in the skin were still significantly increased in STAT3 GOF compared with WT (Fig. S3 D).

Based on accumulation of Th17 cells with STAT3 GOF and lack of requirement of other T cells, we hypothesized that CD4$^+$

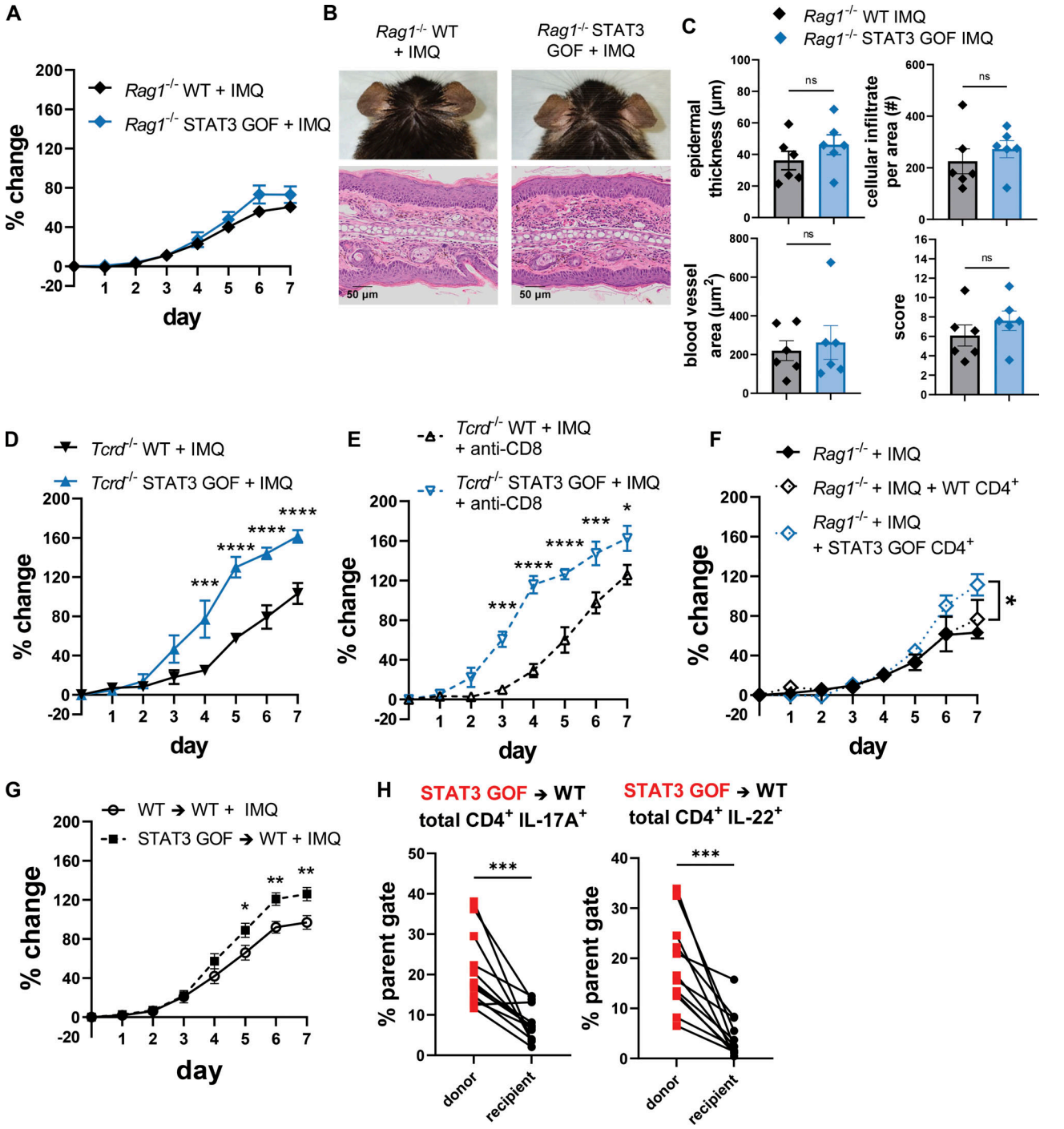

Figure 4. **CD4⁺ T cells are sufficient, and γδ T cells and CD8⁺ T cells are not required to mediate IMQ-induced inflammation in STAT3 GOF mice.** **(A)** Percent change in ear thickness of IMQ-treated *Rag1*$^{-/-}$ mice. **(B)** Representative images of ears and H&E sections of IMQ-treated *Rag1*$^{-/-}$ mice. **(C)** Histological measurements from ears of IMQ-treated *Rag1*$^{-/-}$ mice. **(D)** Percent change in ear thickness of IMQ-treated *Tcrd*$^{-/-}$ mice. **(E)** Percent change in ear thickness of IMQ-treated CD8-depleted *Tcrd*$^{-/-}$ mice. **(F)** Percent change in ear thickness of IMQ-treated *Rag1*$^{-/-}$ mice that received 5 × 10^6 WT or STAT3 GOF CD4⁺ T cells. **(G)** Percent change in ear thickness of IMQ-treated STAT3 GOF → WT BM chimeras. **(H)** Quantification of donor and recipient-derived CD4⁺ IL-17A⁺ and IL-22⁺ frequencies in IMQ-treated STAT3 GOF → WT skin by flow cytometry. Bars: mean ± SEM. Statistical significance was determined by two-way repeated measures ANOVA with Šídák's multiple comparisons test (A and D–G) or unpaired two-tailed or Welch's *t* test (C and H). *P < 0.05, **P < 0.01, ***P < 0.001, ****P < 0.0001. Data represent three to four experiments with 4–12 mice/group. Percent changes in ear thickness are relative to baseline.

T cells were key mediators of inflammation in this model. To test if STAT3 GOF in CD4⁺ T cells could drive skin inflammation, WT or STAT3 GOF CD4⁺ T cells from IMQ-treated IL-17-GFP reporter mice were adoptively transferred into *Rag1*$^{-/-}$ hosts and recipients were treated with IMQ 24 h later. STAT3 GOF CD4⁺ T cells induced greater ear swelling than WT CD4⁺ T cells (Fig. 4 F), which was associated with increased macrophages and decreased DCs/Langerhans cells in the skin compared with

control *Rag1*$^{-/-}$ (Fig. S3 E). Transferred STAT3 GOF CD4$^+$ T cells had reduced expression of Foxp3 and increased expression of IL-22, but IL-17 expression was not significantly different (Fig. S3 F). Together, these data indicate that STAT3 GOF in CD4$^+$ T cells is pathogenic and is associated with increased IL-22 production.

STAT3 GOF in both skin and immune cells leads to the highest burden of spontaneous skin disease, but STAT3 GOF in bone marrow (BM)–derived cells is sufficient for IMQ-induced Th17 accumulation and ear swelling

STAT3 regulates signals in hematopoietic and non-hematopoietic cells and is particularly important for proliferation in somatic cells (Gharibi et al., 2020; Yu et al., 2009). In the skin, IL-22 activates STAT3 signaling in keratinocytes to inhibit differentiation and promote proliferation (Eyerich et al., 2017). Patients with STAT3 GOF syndrome have germline disease, suggesting that organ-specific disease may depend, in part, on STAT3 function in non-hematopoietic cells. To test this, BM chimeras were generated. WT mice received BM from STAT3 GOF mice (STAT3 GOF→WT) and vice versa (WT→STAT3 GOF), with syngeneic controls (WT→WT and STAT3 GOF→STAT3 GOF). While STAT3 GOF→WT chimeras had near complete engraftment in all immune cell types tested in the peripheral blood at 12 wk after transplant, WT→STAT3 GOF recipients unexpectedly had incomplete engraftment in the blood, particularly in the myeloid compartment (Fig. S4, A and B). Control STAT3 GOF→STAT3 GOF also had near complete engraftment in the blood (Fig. S4, A and B). These results demonstrate a defect in engraftment of WT→STAT3 GOF BM chimeras, which resulted in chimeras of mixed nature. Failure of WT BM to engraft in STAT3 GOF hosts was unexpected but may provide some insight into the variable success rates of hematopoietic stem cell transplantation (HSCT) in patients with STAT3 GOF (Leiding et al., 2023).

Spontaneous skin inflammation did not occur in STAT3 GOF→WT mice 12 wk after transplant (Fig. S4 C), suggesting that hematopoietic cells are not sufficient for spontaneous disease. STAT3 GOF recipients did develop spontaneous ear swelling, which was greatest in STAT3 GOF→STAT3 GOF compared with the WT→STAT3 GOF mixed chimera (Fig. S4 C), suggesting that the combination of STAT3 GOF in hematopoietic and non-hematopoietic cells leads to the highest disease burden.

We focused IMQ studies on the STAT3 GOF→WT chimera due to the mixed nature of the WT→STAT3 chimera. Mice were treated with IMQ at 12 wk after transplant. Ear thickness was increased in STAT3 GOF→WT compared with WT→WT chimeras (Fig. 4 G). Increased ear thickness coincided with increased pathological score driven by an increase in cellular infiltrate, but not epidermal thickness (Fig. S4 D). This suggests STAT3 GOF in hematopoietic cells affects recruitment of immune cells but the epidermal hyperplasia seen in older germline STAT3 GOF mice may be due to STAT3 GOF in the epidermal cells. Analysis of cytokine production in donor-derived T cells revealed an increase in the frequency of IL-17A$^+$ and IL-22$^+$ CD4$^+$ T cells in the STAT3 GOF → WT, demonstrating that the Th17 response is cell intrinsic (Fig. 4 H).

In summary, BM chimeras revealed that the IMQ-induced Th17 response was intrinsic to STAT3 GOF–expressing T cells, which were sufficient to drive IMQ-induced inflammation, but not increased epidermal thickness. Spontaneous skin disease required the presence of STAT3 GOF in non-hematopoietic cells, suggesting that STAT3 GOF expression in epithelial cells plays an important role in disease in this model and likely in patients.

STAT3 GOF CD4$^+$ T cells show increased clonal expansion at baseline and after IMQ

IMQ-treated STAT3 GOF mice showed an enhanced Th17 response in the CLN as demonstrated by the increased frequency and number of IL-22$^+$ CD4$^+$ T cells and increased total numbers of IL-17A$^+$ CD4$^+$ T cells. To examine transcriptional changes caused by STAT3 GOF in T cells and determine if STAT3 GOF drives increased clonal expansion, cellular indexing of transcriptomes and epitopes sequencing (CITE-seq) (Stoeckius et al., 2017) with TCR-seq was performed on enriched CD3$^+$ cells from the CLN of young adult WT and STAT3 GOF littermates with and without IMQ treatment. A multimodal uniform manifold approximation and projection (UMAP) projection of 54 clusters across 135,567 cells from all conditions was generated using weighted nearest neighbor analysis of RNA and surface protein expression (Fig. 5 A) (Hao et al., 2021). Clustering remained similar between genotype and treatment (Fig. 5 B). However, multiple clusters (1, 6, 10, 16, 24, 29, 39, 42, 45, and 52) were enriched in STAT3 GOF cells (Fig. 5 C). Clusters of either single-positive CD4 or CD8 T cells were selected based on antibody expression (which matched gene expression) and then reclustered and manually annotated based on protein expression of CD44 and CD62L, and by gene signatures (Fig. 5 D and Fig. S5 A, see Materials and methods for clustering signatures used). T cells were identified as naïve, effector/effector memory (Eff/TEM), central memory (TCM), exhausted (Exh), and Tregs (CD4$^+$ T cells only) or intermediate (Int, CD8$^+$ T cells only) (Fig. 5, D and E; and Fig. S5, A and B). CD4$^+$ TCM and Exh clusters with no treatment (NT) and the IMQ CD4$^+$ TCM and Treg clusters showed trends of increased frequencies in STAT3 GOF samples (Fig. 5 E). Similarly, the CD8$^+$ TCM cluster trended toward increased frequency in NT STAT3 GOF samples compared with WT, suggesting that STAT3 GOF T cells have encountered antigen at baseline (Fig. S5 B).

Next, transcriptional differences in CD4$^+$ T cells by annotated cluster were examined. At baseline, STAT3 target genes (*Socs3*, *Maf*, *Cxcr3*) were upregulated in the TCM cluster of STAT3 GOF CD4$^+$ T cells (Fig. 5 F), consistent with a phenotype of increased STAT3 signaling in this model. Calcium binding genes (*S100a4*, *S100a6*, and *S100a11*), which were induced by STAT3-activating cytokines IL-6 and IL-11 in vitro (Al-Ismaeel et al., 2019), were also upregulated in the STAT3 GOF CD4$^+$ TCM cluster (Fig. 5 F). Notably, T follicular helper cell (TFH) genes such as *Il21* and *Cxcr5*, and exhaustion and inflammatory genes such as *Tigit*, *Tox2*, *S100a6*, and *S100a11* were upregulated in the STAT3 GOF NT Exh cluster (Fig. 5 G), suggesting that these cells have features of both TFH and exhausted cells. Several Th17-related genes were upregulated in the STAT3 GOF IMQ Eff/TEM cluster, including *Il17a*, *Il17f*, *Il22*, *Ccr6*, and *Rora*, consistent with flow

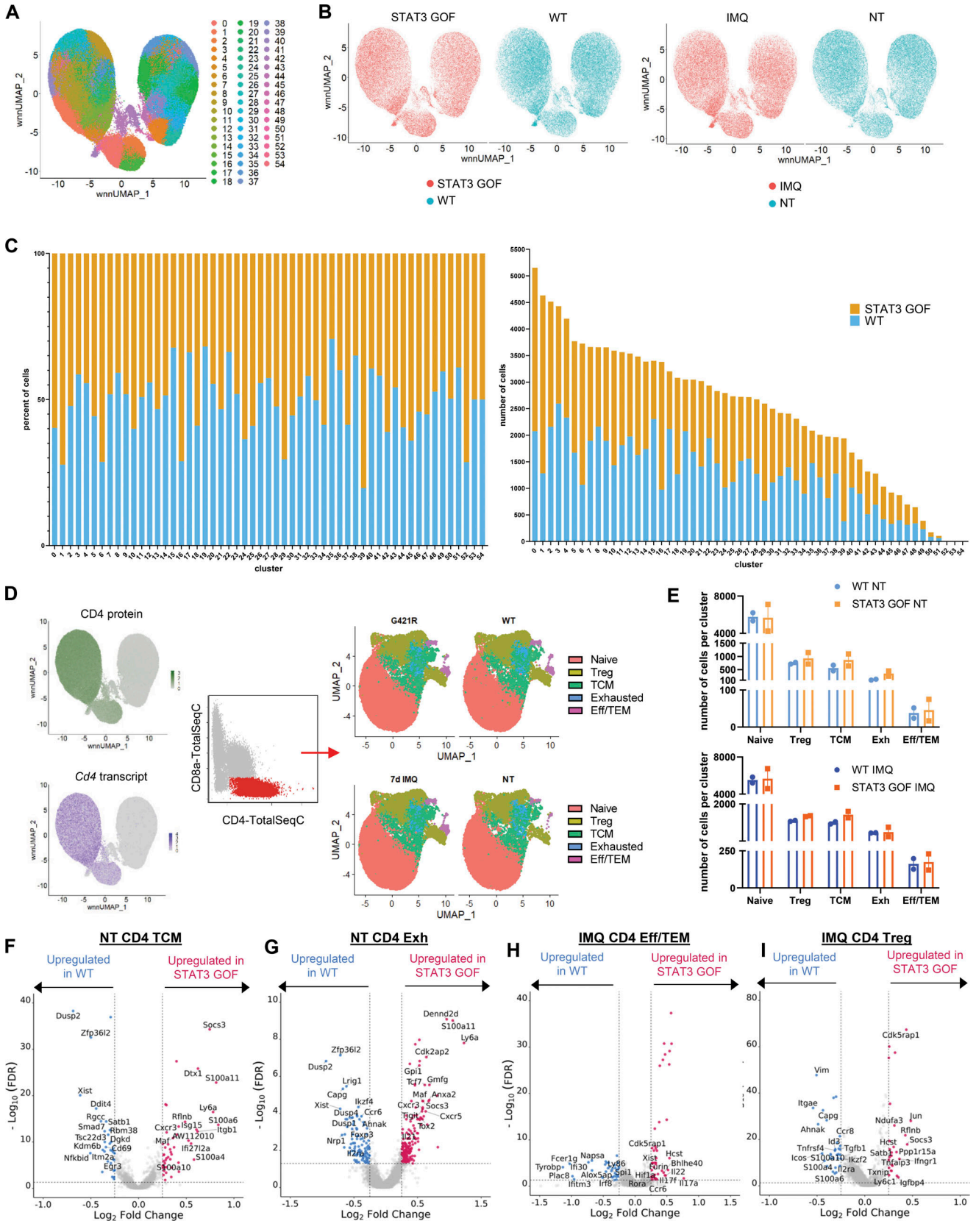

Figure 5. **T cell scRNA-seq with and without IMQ treatment. (A and B)** (A) UMAP projection of CD3⁺ T cells from CLN of NT or IMQ-treated mice (n = 2/group) used in CITE-seq experiment showing unique clusters and (B) sample identity by genotype and treatment. **(C)** Number of cells in each cluster by genotype. **(D)** Single-positive CD4 T cells separated by Cellselector function, then renormalized and reclustered based on CD44 and CD62L surface expression and canonical gene expression. **(E)** Frequencies of NT (top) and IMQ (bottom) annotated CD4⁺ clusters. **(F–I)** Volcano plots showing differential expression

comparing WT and STAT3 GOF (false discovery rate [FDR] < 0.05, average $\log_2$ fold change >0.25 or less than −0.25) in cells identified as NT TCM (F), NT Exh, (G), IMQ Eff/TEM (H), and IMQ Treg (I). Ribosomal genes, genes ending in -Rik, and genes beginning with Gm- are not labeled in volcano plots. Data are representative of one experiment with two mice/group.

cytometry data (Fig. 5 H). In the IMQ Treg cluster, STAT3 targets (*Jun*, *Socs3*) and *Satb1*, which have been shown to alter pTreg differentiation (Kitagawa et al., 2017), were upregulated in STAT3 GOF. Upregulated genes in WT NT Tregs included *Ikzf2*, *Il2ra*, and *Tgfb1* (Fig. 5 I), suggesting an altered local Treg phenotype in STAT3 GOF with this model.

These data suggest CD4+ T cells are important for disease, thus clonal expansion in STAT3 GOF CD4+ T cells was compared with WT. At baseline, STAT3 GOF CD4+ T cells showed an increased clonal response in the TCM, Exh, and to a minor extent Treg clusters based on the presence of medium-sized clones (defined as 5–20 clones) (Fig. 6 A). Clonal expansion was increased in STAT3 GOF IMQ Eff/TEM and TCM clusters compared to WT; however, clonal expansion was diminished in the STAT3 GOF IMQ Treg cluster (Fig. 6 A), perhaps indicative of impaired pTreg generation or recruitment.

Expanded CD4+ clones from NT STAT3 GOF showed upregulation of genes regulated by STAT3 (*Socs3*, *Cxcr5*, and *Maf*), STAT3 binding partners (*Junb*), and exhaustion-related genes (*Tox*, *Tox2*) (Fig. 6 B), providing additional evidence for a persistent stimulus in STAT3 GOF at baseline. Following IMQ treatment, expanded CD4+ clones showed upregulation of *Socs3*, *Junb*, *Fos*, and *Il22*, while WT clones showed upregulation of Treg-related genes including *Foxp3*, *Il2ra*, and *Ikzf2* (Fig. 6 C). This suggests that expanded CD4+ clones in STAT3 GOF have a Th17 phenotype and may be less likely to be Tregs. Interestingly, STAT3 GOF expanded clones from the Treg cluster upregulated *Il22* (Fig. 6 D). These transcriptional profiles were not observed in single clones of total IMQ CD4+ T cells (Fig. 6 E), single clones of the IMQ Eff/TEM cluster (Fig. 6 F), or single clones of the IMQ Treg cluster (Fig. 6 G). Thus, Th17 features in STAT3 GOF CD4 T cells and Treg features in WT CD4 T cells appear to be specific to expanded clones. Together, the diminished clonal expansion, Th17-like gene expression, and the observations of upregulated *Ikzf2*, *Il2ra*, and *Tgfb1* in WT Tregs compared with STAT3 GOF suggest that STAT3 GOF could alter local Treg phenotype during skin inflammation.

Two recent studies found increased clonal expansion of CD8+ T cells in STAT3 GOF mice that was associated with disease (Masle-Farquhar et al., 2022; Warshauer et al., 2021). While CD8+ T cells were not required for skin inflammation in our model, there was increased CD8+ clonal expansion at baseline in STAT3 GOF Eff/TEM, TCM, and Int clusters (Fig. S5 C). IMQ-treated STAT3 GOF CD8+ T cells showed increased clonal expansion of TCM and Int clusters with the emergence of large-sized clones (defined as 20–100 clones), but fewer Eff/TEM clones (Fig. S5 C). These data suggest that T cells in STAT3 GOF are more likely to be activated or antigen-experienced at baseline, which could contribute to the increased clonal response following stimulation. Genes involved in effector T cell cytotoxicity and chemotaxis (*Ccl5*, *Ccr5*, *Ccl4*, *Ctla2a*, *Gzmk*, *Eomes*, *Nkg7*, and *Gzmb*) were upregulated in both NT and IMQ-treated STAT3 GOF expanded CD8+ clones compared with WT(Fig. S5, D and E), consistent with previous analyses of STAT3 GOF CD8+ T cell transcript profiles in other disease models (Masle-Farquhar et al., 2022; Warshauer et al., 2021).

IL-22 signaling contributes to increased inflammation in STAT3 GOF

Given the observation of expanded IL-22–expressing T cells in STAT3 GOF mice, we hypothesized that IL-22 was important for driving enhanced disease (Van Belle et al., 2012). STAT3 GOF mice were crossed to IL-22–deficient (*Il22*$^{-/-}$) mice and examined for spontaneous skin inflammation as they aged. Older adult *Il22*$^{-/-}$ STAT3 GOF mice did not appear to develop ear swelling (Fig. 7 A). There was no neutrophil infiltration into the skin, but the frequency of DCs/Langerhans cells was decreased in *Il22*$^{-/-}$ STAT3 GOF mice similar to that observed in IL-22–replete animals (Fig. 7 B). The total number of CD4+ IL-17A+, but not IL-17A+ γδ T cells, was increased in the skin of *Il22*$^{-/-}$ STAT3 GOF mice (Fig. 7 C). A similar pattern was observed in the CLN (Fig. 7, D and E). We next treated young adult *Il22*$^{-/-}$ and *Il22*$^{-/-}$ STAT3 GOF mice with IMQ. Ear swelling in *Il22*$^{-/-}$ STAT3 GOF mice was reduced to levels similar to IL-22–sufficient WT mice (Fig. 8 A). However, *Il22*$^{-/-}$ STAT3 GOF mice had increased ear swelling compared with *Il22*$^{-/-}$ WT mice (Fig. 8 A), with corresponding increased epidermal thickness, cellular infiltrate count, and pathological score (Fig. 8, B and C). The frequency and number of skin-infiltrating neutrophils were both increased, while the frequency of DCs/Langerhans cells was decreased in *Il22*$^{-/-}$ STAT3 GOF mice (Fig. 8 D). Additionally, the frequency and number of skin IL-17A+ CD4+ T cells continued to be higher in the skin of STAT3 GOF compared with *Il22*$^{-/-}$ WT mice (Fig. 8 E). In the CLN, total cellularity was higher in *Il22*$^{-/-}$ STAT3 GOF (Fig. 8 G), corresponding with an increased total number of IL-17A+ CD4+ T cells (Fig. 8 H) and IL-17A+ γδ T cells (Fig. 8 I). We hypothesized that increased IL-17A frequency may explain the continued small but significant difference in ear swelling and neutrophil infiltration; however, depletion of IL-17A in *Il22*$^{-/-}$ mice during IMQ treatment did not affect the difference in ear swelling (Fig. 8 J). Collectively, these data demonstrate that IL-22, which is enhanced in STAT3 GOF CD4+ T cells, partially mediates skin disease in STAT3 GOF and likely plays a large role in driving STAT3 activation in non-hematopoietic cells following IMQ. However, it is important to note that other factors still contribute to the increased neutrophil infiltration and histological changes in the skin, which combined with IL-22 signaling can drive the full disease phenotype.

JAK inhibition prevents enhanced IMQ-induced inflammation in STAT3 GOF without affecting local Th17 response

JAKinibs have been used alone or in conjunction with IL-6R antagonists to treat STAT3 GOF patients, including those with

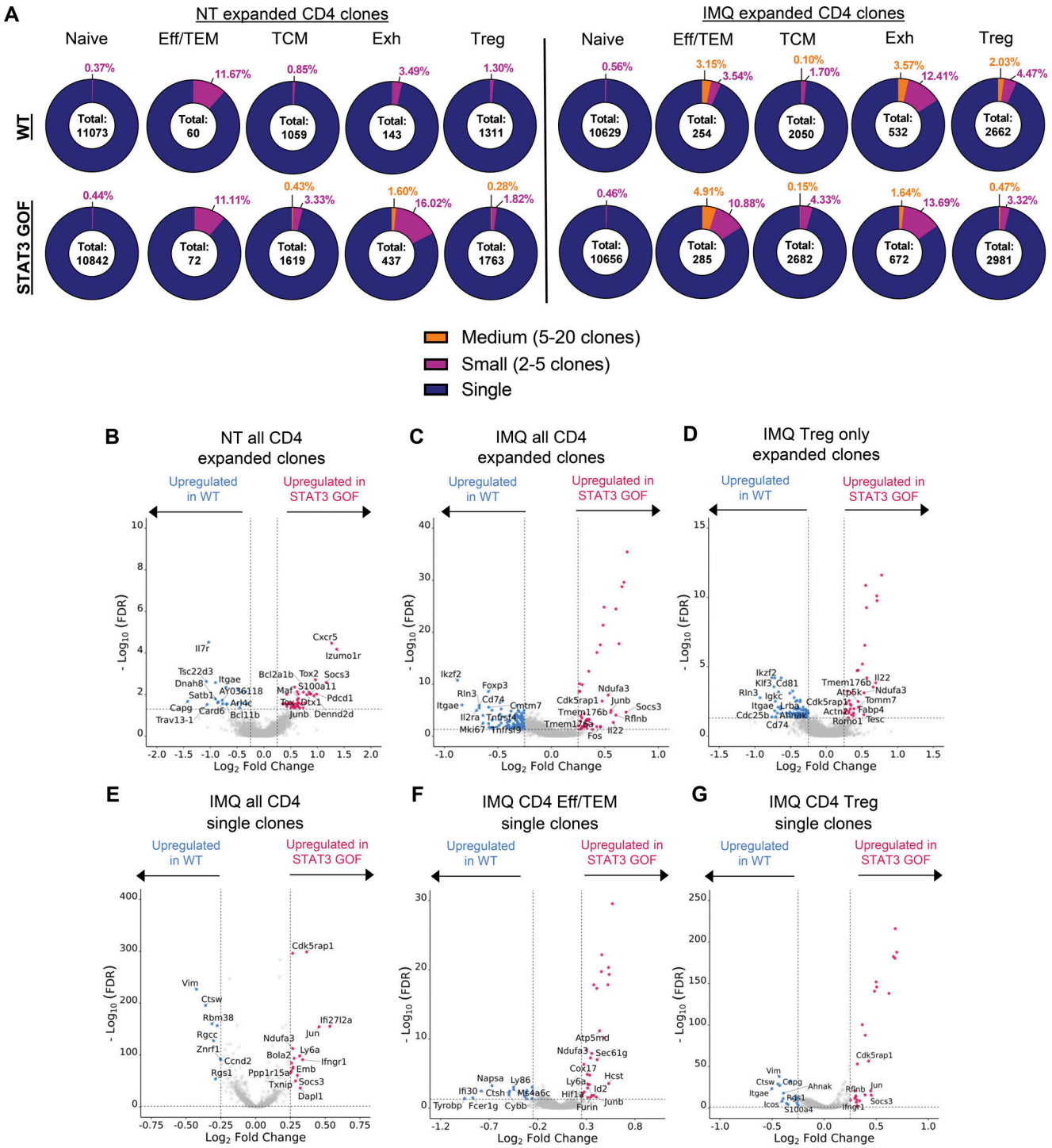

Figure 6. **STAT3 GOF CD4⁺ T cells show increased clonal expansion at baseline and after IMQ. (A)** Clonotype frequency of NT and IMQ-treated CD4⁺ T cells by annotated cluster used in scRNA-seq experiment, generated with ScRepertoire. **(B–D)** Volcano plot showing differential expression comparing WT and STAT3 GOF (FDR < 0.05, average $\log_2$ fold change >0.25 or less than −0.25) in NT CD4⁺ expanded clones (B), IMQ CD4⁺ expanded clones (C), and IMQ Treg expanded clones (D). **(E–G)** Volcano plot showing differential expression comparing WT and STAT3 GOF (FDR < 0.05, average $\log_2$ fold change >0.25 or less than −0.25) in IMQ CD4⁺ single clones (E), IMQ CD4⁺ Eff/TEM single clones (F), and IMQ CD4⁺ Treg single clones (G). Ribosomal genes, genes ending in -Rik, and genes beginning with Gm- are not labeled in volcano plots. Data are representative of one experiment with two mice/group.

the p.G421R variant (Forbes et al., 2018). To determine if JAK-inibs could reduce IMQ-induced inflammation in STAT3 GOF mice, young adult mice were simultaneously treated with JAK-inib (oral tofacitinib, a JAK1/3 inhibitor) and IMQ for 7 days. Treatment with tofacitinib reduced disease as measured by ear thickness in both WT and STAT3 GOF mice, with ear thickness in JAKinib-treated STAT3 GOF mice reduced to that of IMQ-treated WT mice (Fig. 9 A). JAKinib-treated STAT3 GOF mice

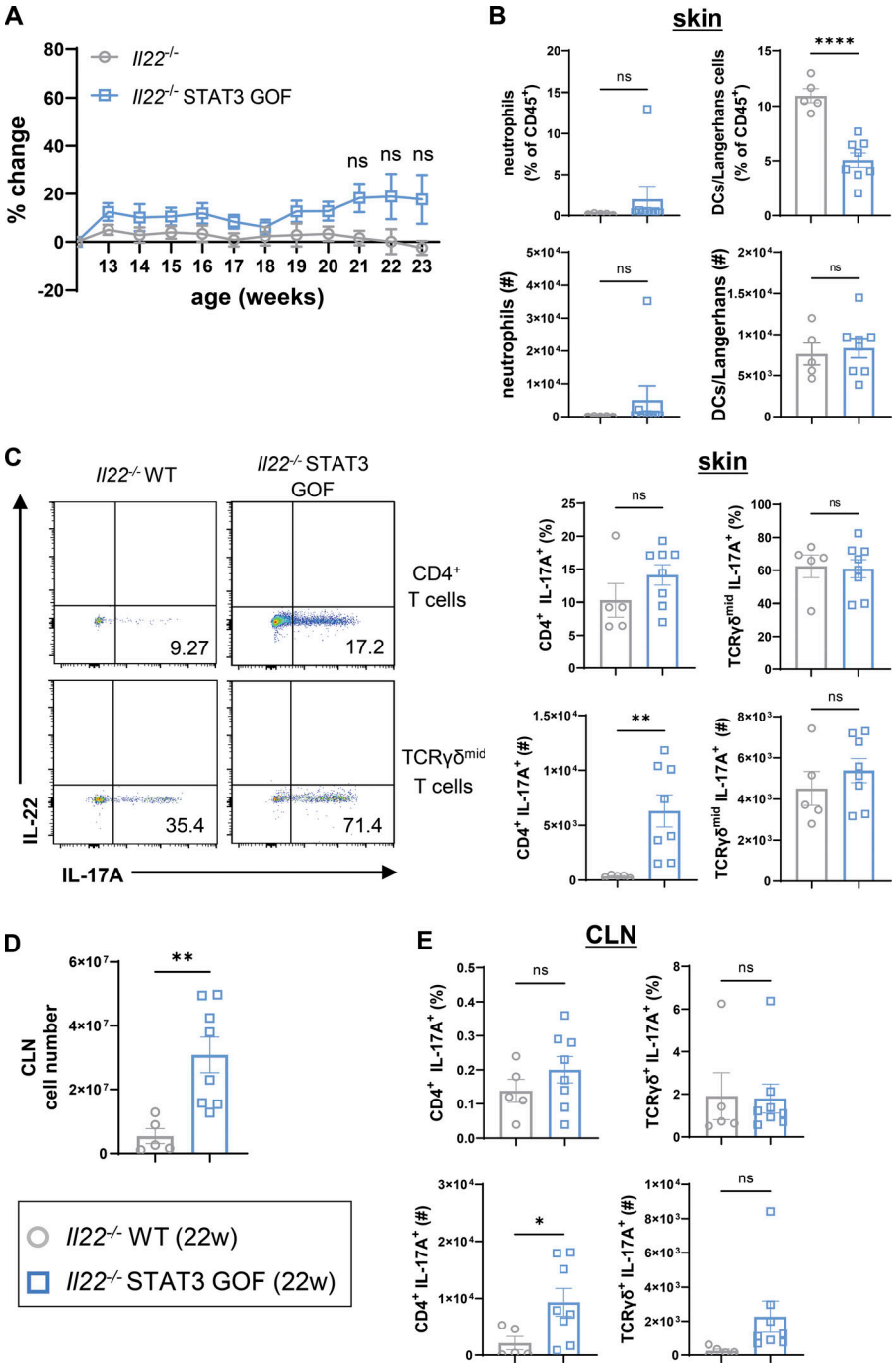

Figure 7. **Older adult *Il22*$^{-/-}$ STAT3 GOF mice do not develop spontaneous skin inflammation. (A)** Percent change in ear thickness of older adult *Il22*$^{-/-}$ and *Il22*$^{-/-}$ STAT3 GOF mice relative to baseline at 13 wk. **(B)** Quantification of skin immune cell frequencies by flow cytometry at 23 wk of age. **(C)** Representative flow plots and quantification of IL-17A$^+$ CD4$^+$ and γδ T cell frequencies and total number in the skin. Cytokines assessed after PMA/ionomycin stimulation. **(D)** Total cellularity of CLN. w, week. **(E)** Quantification of IL-17A$^+$ CD4$^+$ and γδ T cell frequencies and total number in the CLN. Cytokines assessed after PMA/ionomycin stimulation. Bars: mean ± SEM. Statistical significance determined by unpaired two-tailed or Welch's *t* test (B–E), or two-way repeated measures ANOVA with Šídák's multiple comparisons test (A), *P < 0.05, **P < 0.01, ****P < 0.0001. Data are representative of one experiment with five to eight mice/group.

also had significantly improved epidermal thickness, cellular infiltrate, and overall pathological score compared with IMQ-only treated STAT3 GOF, with pathology similar to that seen in IMQ-treated WT mice (with or without JAKinib) (Fig. 9, B and C). These findings demonstrate that JAK inhibition can treat IMQ-induced skin inflammation in STAT3 GOF mice but has a minimal effect on WT mice.

Unexpectedly, JAKinib treatment resulted in increased keratinocyte proliferation as measured by Ki-67$^+$ cells in the epidermis for both WT and STAT3 GOF (Fig. 9 D). Given the overall decrease in epidermal thickness with JAKinib treatment, increased turnover in epithelial cells may be due to processes involved with the resolution of inflammation or other proliferative mechanisms that do not rely on JAK1/3-STAT3 signaling. Neutrophil and monocyte infiltration in the skin was also decreased in STAT3 GOF with JAKinib treatment, while DC/Langerhans cell frequencies were increased in both treated WT and STAT3 GOF (Fig. 9 E), indicating that immune cell recruitment to the skin is altered by tofacitinib. By contrast, IL-17A$^+$ and IL-22$^+$ CD4$^+$ T cells persisted in STAT3 GOF mice following JAKinib treatment, suggesting no effect on local recruitment and/or expansion of these cells with tofacitinib (Fig. 9 F).

These findings demonstrate that treatment with JAKinib improves skin disease in STAT3 GOF. It leads to improved skin

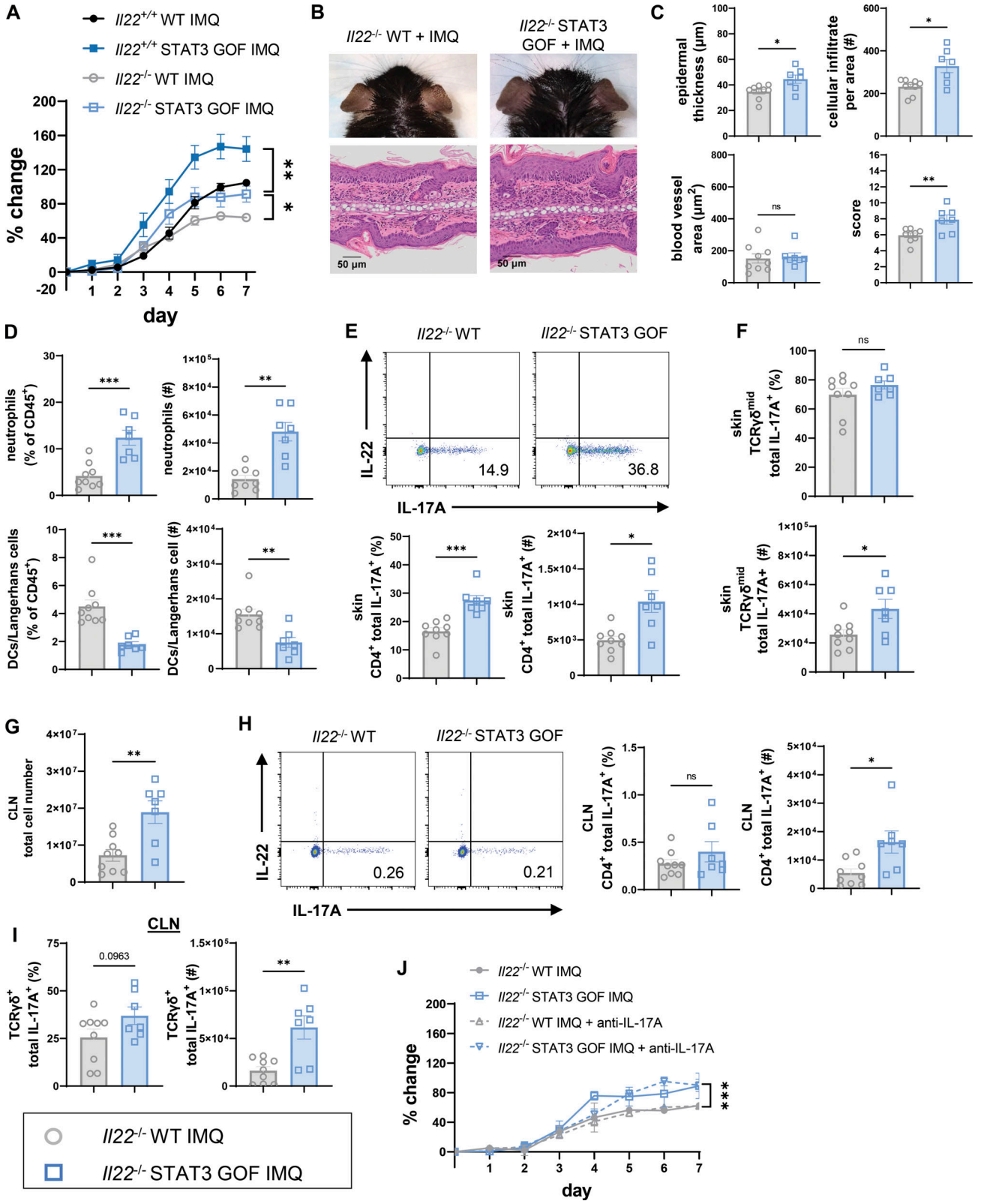

Figure 8. **IL-22 signaling contributes to increased IMQ-induced inflammation in STAT3 GOF. (A)** Percent change in ear thickness of *Il22*$^{+/+}$ and *Il22*$^{-/-}$ WT and STAT3 GOF mice during IMQ treatment relative to baseline. Day 7 statistics shown (top: *Il22*$^{+/+}$ STAT3 GOF versus *Il22*$^{-/-}$ STAT3 GOF; bottom: *Il22*$^{-/-}$ WT versus *Il22*$^{-/-}$ STAT3 GOF). **(B)** Representative images of ears and H&E sections of IMQ-treated *Il22*$^{-/-}$ mice. **(C)** Histological measurements from ears. **(D)** Frequency and quantification of skin immune cells measured by flow cytometry. **(E)** Representative flow plot and quantification of IL-17A expression and total cell number of skin CD4^{+} T cells. Cytokines assessed after PMA/ionomycin stimulation. **(F)** Quantification of IL-17A expression and total cell number of skin γδ T cells. Cytokines assessed after PMA/ionomycin stimulation. **(G)** Total CLN cell number. **(H)** Representative flow plot and quantification of IL-17A

expression and total cell number of CLN CD4+ T cells measured by flow cytometry. Cytokines assessed after PMA/ionomycin stimulation. **(I)** Quantification of IL-17A expression and total cell number of CLN γδ T cells measured by flow cytometry. Cytokines assessed after PMA/ionomycin stimulation. **(J)** Percent change in ear thickness of IL-17A–depleted *Il22*$^{-/-}$ WT and STAT3 GOF mice during IMQ treatment relative to baseline. Day 7 statistics shown (*Il22*$^{-/-}$ WT + anti-IL-17A versus *Il22*$^{-/-}$ STAT3 GOF + anti-IL-17A). Bars: mean ± SEM. Statistical significance was determined by two-way repeated measures ANOVA with Tukey's multiple comparisons test (A and J) or unpaired two-tailed or Welch's *t* test (D–I). *P < 0.05, **P < 0.01, ***P < 0.001. Data are representative of two independent experiments with 6–11 mice/group.

pathology, decreased recruitment of innate immune cells, and enhanced keratinocyte proliferation. However, it does not alter the population of skin Th17 cells. By contrast, in WT mice tofacitinib led to a mild reduction in ear swelling, but no changes in pathologic score or neutrophil infiltration, supporting differences in disease pathology due to STAT3 GOF.

These findings also provide strong supportive evidence for investigating local inflammatory responses and pathology in both immune cells and affected tissue with STAT3 GOF syndrome. Finally, the response to JAKinib therapy in STAT3 GOF, but not WT mice, further supports the use of mechanism-based therapies that specifically target STAT3 GOF, or other monogenic IEI, despite minimal efficacy for more common diseases with similar pathologic features.

Discussion

Here, we demonstrate spontaneous and stimulus-driven skin disease in a mouse model harboring a pathogenic human STAT3 variant (p.G421R) associated with a local cell-intrinsic Th17 response. CD4+ T cells are sufficient to drive increased ear swelling in STAT3 GOF mice following topical IMQ, and disease does not require γδ or CD8+ T cells. CITE-seq revealed enhanced clonal CD4+ T cell responses in STAT3 GOF and increased expression of STAT3-regulated genes, including *Il22*, in IMQ-treated expanded clones. IL-22–deficient STAT3 GOF mice had improved ear swelling, but persistent infiltration of IL-17A+ CD4+ T cells. JAKinib treatment improved clinical disease and was associated with reduced neutrophil influx, increased DCs in the skin, and keratinocyte proliferation, but did not alter Th17 cell infiltration.

Increased Th17 responses in the peripheral blood have not been demonstrated in all patients with STAT3 GOF (Leiding et al., 2023). Nevertheless, normalization of Th17 frequencies following tocilizumab was associated with disease improvement in two patients with the p.G421R variant and another with the p.P471R variant (Khoury et al., 2017; Milner et al., 2015; Wienke et al., 2015). Here, both spontaneous and IMQ-induced skin disease were associated with a local Th17 response (skin) and systemic (CLN and spleen) IL-22 response. This suggests that peripheral blood analysis may not reflect organ-specific inflammation in patients.

Accumulation of Th17 cells with skin inflammation was unique to STAT3 GOF mice and not seen in WT littermates. The initial trigger for inflammation with spontaneous disease is unknown, but we hypothesize that it is due to chronic STAT3 signaling associated with commensal microbiota at this barrier surface. In the IMQ model, we hypothesize that initial generation of local Th17 responses is due to induction of IL-6 and other cytokines. We observed increased *Ccr6* expression in effector CD4 T cells in STAT3 GOF CLN with IMQ by single-cell RNA-seq (scRNA-seq), suggesting altered homing to inflamed tissues in STAT3 GOF. Both spontaneous and IMQ-induced inflammation was associated with increased total IL-17A+, total IL-22+, and IL-17A+ IL-22+ double-positive CD4+ and γδ T cells in the skin of STAT3 GOF mice. STAT3 transcriptional activity leads to IL-17A and IL-22 expression in CD4+ T cells and γδ T cells through activating cytokines including IL-23 and IL-21 (Guo et al., 2014; Liang et al., 2006; Sutton et al., 2009; Yeste et al., 2014; Zheng et al., 2007). Our data suggest that Th17 cells are the major source of these cytokines in STAT3 GOF; however, a role for Th22 cells is not excluded since we have observed a significant increase in local and peripheral IL-22–expressing CD4+ T cells. Interestingly, lineage tracing of T cells in a recent study found that IL-22 single-positive T cells can develop from ex-Th17 (Barnes et al., 2021). Given the importance of STAT3 in the development of both Th22 and Th17, both cell types may be contributing to the phenotype in this model and both may exhibit plasticity.

The IL-22 receptor signals through STAT3 in keratinocytes and upregulates genes involved in keratinocyte proliferation and expression of CCL20 (Eyerich et al., 2017; Harper et al., 2009; Wolk et al., 2004, 2006). Deletion of *Il22* improved disease with IMQ, but there was persistent increased epidermal thickness. Possible explanations include IL-17R signaling in keratinocytes, which can also drive proliferation and secretion of chemokines that recruit neutrophils (Moos et al., 2019). A previous study in *Il22*$^{-/-}$ mice showed that IL-17A+ CD4 T cells increased with IMQ, suggesting a compensatory mechanism that enhances IL-17A production in the absence of IL-22 (Tortola et al., 2012). This compensation may be further exaggerated by STAT3 GOF given the increased IL-17A expression in skin *Il22*$^{-/-}$ γδ T cells after IMQ.

There is a diverse clinical phenotype in patients with STAT3 GOF, even among individuals with the same genetic variant (Leiding et al., 2023). Similarly, mouse models of STAT3 GOF from our group and others have phenotypic differences, likely due to different environmental and genetic factors, including genetic background and heterozygous or homozygous state of the STAT3 GOF variants (Masle-Farquhar et al., 2022; Schmitt et al., 2022; Warshauer et al., 2021). In a model from Warshauer et al. (2021), the p.K392R variant (also in the DNA binding domain) on the NOD background led to accelerated diabetes in heterozygous mice, driven by clonally expanded effector CD8+ T cells that resisted terminal exhaustion. In a separate study, mice with the p.K392R variant on the C57BL/6 background had progressive lymphoproliferation with increased Th17 differentiation in vitro and in a model of induced experimental autoimmune encephalomyelitis, but no difference in clinical disease

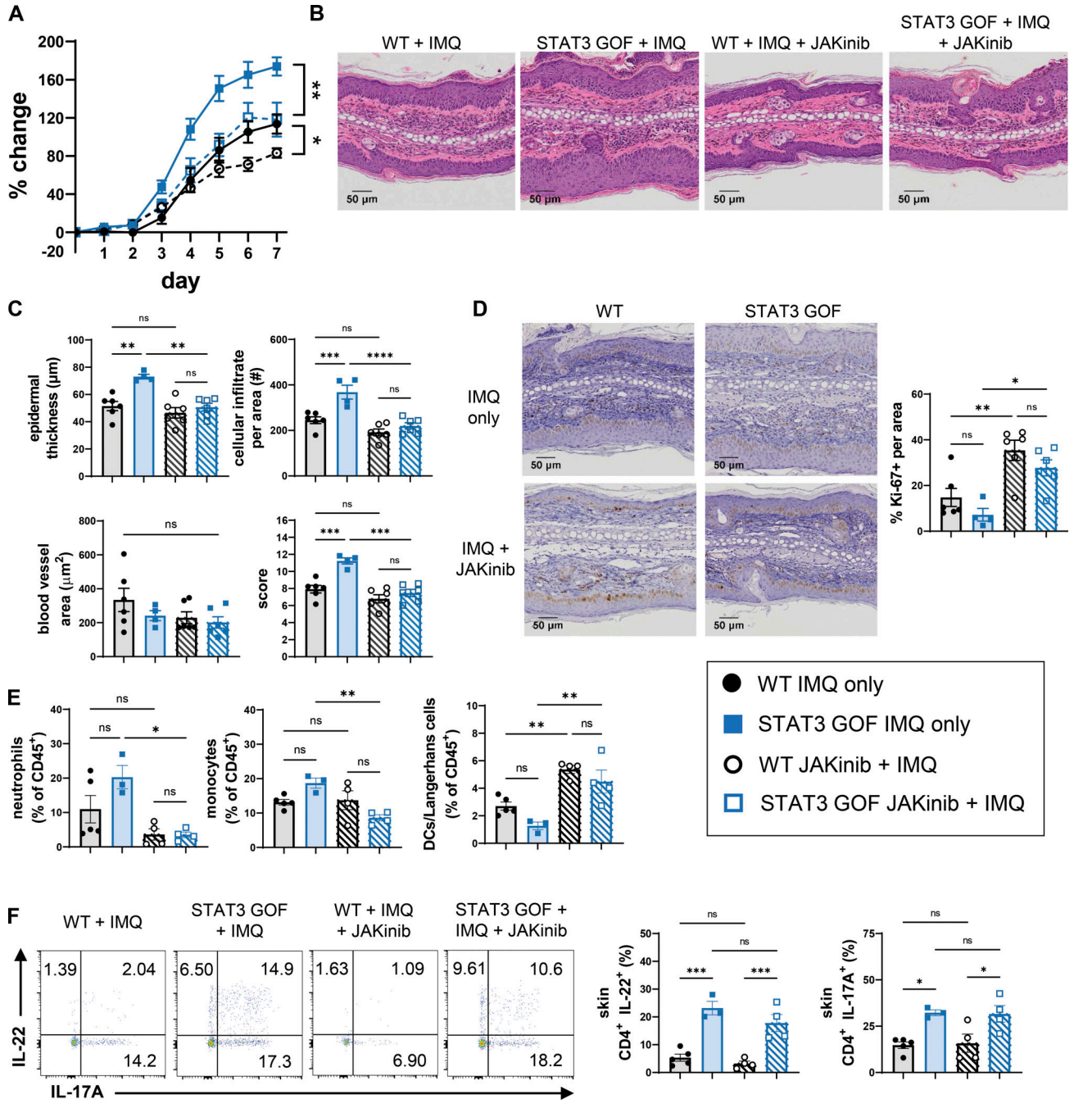

Figure 9. **JAK inhibition prevents enhanced inflammation in STAT3 GOF caused by IMQ without affecting Th17 cytokine expression.** WT and STAT3 GOF littermates received JAKinib (tofacitinib) delivered in chow. IMQ treatment started on the same day. **(A)** Percent change in ear thickness during IMQ treatment relative to baseline. Day 7 statistics are shown. **(B)** Representative images of H&E ear sections. **(C)** Histological measurements from H&E ear sections. **(D)** Representative images of Ki-67–stained ear sections with quantification. **(E)** Quantification of skin immune cells measured by flow cytometry. **(F)** Representative flow plot and quantification of IL-17A and IL-22 expression in skin CD4⁺ T cells. Cytokines assessed after PMA/ionomycin stimulation. Bars: mean ± SEM. Statistical significance determined by two-way repeated measures ANOVA with Šídák's multiple comparisons test (A) or one-way ANOVA with Šídák's multiple comparisons test (B–F). *P < 0.05, **P < 0.01, ***P < 0.001, ****P < 0.0001. Data are representative of two experiments with three to six mice/group.

(Woods et al., 2022). Masle-Farquhar et al. (2022) reported two models on the C57BL/6 background, including p.K658N, a variant associated primarily with somatic mutations in large granular lymphocytic (LGL) leukemia, and p.T716M, associated with STAT3 GOF syndrome. Both models had lymphoproliferation in the heterozygous and homozygous state, mediated by dysregulated oligoclonal effector CD8⁺ T cells resembling T-LGL cells (Masle-Farquhar et al., 2022). Similar to other models, mice homozygous for STAT3 GOF had runting and early death due to an uncertain cause (Masle-Farquhar et al., 2022; Schmitt et al.,

2022; Woods et al., 2022). Transplantation of homozygous STAT3 GOF BM into *Rag1*$^{-/-}$ recipients demonstrated cell-intrinsic CD8$^+$ T cell expansion and led to fatal disease with lymphoproliferation and wasting that was alleviated by CD8$^+$ T cell depletion (Masle-Farquhar et al., 2022). Interestingly, spontaneous skin inflammation was observed in aged homozygous mice, although neither etiology nor skin immune cells were examined in these models (Masle-Farquhar et al., 2022). Our data using the p.G421R variant showed that CD8$^+$ T cells are not required for increased skin inflammation in STAT3 GOF, as ear swelling was not affected by CD8$^+$ depletion in γδ T cell KO mice. In line with other STAT3 GOF models, expanded CD8$^+$ clones had increased expression of cytotoxic genes, demonstrating baseline CD8$^+$ T cell dysregulation (Masle-Farquhar et al., 2022; Warshauer et al., 2021). Differences between STAT3 GOF models highlight the unique genetic, environmental, and cellular requirements for different disease phenotypes.

We previously reported T cell dysregulation and lymphoproliferation in older adult STAT3 GOF mice of the p.G421R variant, with expansion of Tregs and Th1 cells, but no differences in splenic IL-17A$^+$ CD4$^+$ T cells (Schmitt et al., 2022). Treg function in vitro was intact with STAT3 GOF; however, peripheral Tregs were decreased and IL-17A$^+$ ex-Tregs were increased in a T cell transfer model of colitis (Schmitt et al., 2022). In lesional skin (and peripheral blood mononuclear cell) of patients with psoriasis, decreased FOXP3 and increased IL-17A expression in Tregs can be driven by STAT3-activating cytokines IL-23 and IL-21 ex vivo (Bovenschen et al., 2011; Shi et al., 2019; Zhou et al., 2009). Here, there were reduced numbers of skin Tregs during inflammation and reduced clonal expansion of STAT3 GOF Tregs with IMQ treatment. Interestingly, *Il22* was upregulated in STAT3 GOF Treg clones with IMQ, and there was also an increase in CD4$^+$ Foxp3$^+$ Rorγt$^+$ IL-17–expressing cells in STAT3 GOF skin with IMQ treatment. Similar populations of FoxP3$^+$ RORγt$^+$ IL-17$^+$ cells have been observed in psoriasis (Bovenschen et al., 2011) and inflammatory bowel disease (Ueno et al., 2013). These data suggest that STAT3 GOF may lead to dysregulated recruitment of Tregs, a lack of induced Tregs at sites of inflammation, as we saw in a model of colitis (Schmitt et al., 2022), or deviation from the canonical Treg phenotype in inflamed tissues.

STAT3 GOF in non-hematopoietic cells can influence skin disease. While STAT3→WT BM chimeras had more severe IMQ-induced disease and cellular infiltrate, they did not have significantly increased epidermal thickness. Spontaneous ear swelling was not seen in STAT3→WT BM chimeras but was found in WT→STAT3 mixed chimeras and most prominently in STAT3→STAT3 chimeras. Indeed, patients with psoriasis have high levels of STAT3 activity in keratinocytes from psoriatic lesions (Miyoshi et al., 2011; Sano et al., 2005), and overexpression of STAT3 in keratinocytes led to spontaneous and wound-induced skin inflammation resembling psoriasis in mice (Sano et al., 2005). It should be noted that certain hematopoietic cell populations in the skin are radioresistant, including tissue-resident γδ T cells, some macrophage populations, and Langerhans cells, and STAT3 GOF in these cell types may be affecting this phenotype. While these BM chimeras demonstrate the importance of STAT3 GOF in the skin, it was not sufficient to drive disease. STAT3 GOF *Rag1*$^{-/-}$ did not have significant ear swelling with IMQ, and adoptive transfer of STAT3 GOF CD4$^+$ T cells was sufficient to induce ear swelling with IMQ, demonstrating pathogenicity of T cells. However, this transfer model did not recapitulate all aspects of disease, again highlighting the importance of STAT3 GOF in both CD4$^+$ T cells and skin epithelial cells for the full clinical phenotype and the need to target multiple cell types in patients. Of note, a recent study found that deletion of *Stat3* in keratinocytes diminished IMQ-induced skin inflammation, but deletion of *Stat3* in T cells had no effect (Ravipati et al., 2022). Nevertheless, disease driven by STAT3 GOF here is distinct from IMQ-induced inflammation in WT mice. For example, STAT3 GOF–driven disease is dependent on CD4$^+$ T cells and not γδ T cells. This is likely due to a combination of the unique inflammatory environment in STAT3 GOF mice with baseline lymphoproliferation and the nature of the GOF variants that drive disease. Overall, these data demonstrate that STAT3 signaling in hematopoietic and non-hematopoietic cells should be considered when designing therapies for patients.

Current best available therapies for STAT3 GOF syndrome include JAKinibs and IL-6R antagonists, which target multiple cell types (Leiding et al., 2023). Our results show that JAK inhibition by tofacitinib, which targets JAK1 and JAK3, does not affect enhanced Th17 responses in STAT3 GOF, but ameliorates disease and increases keratinocyte proliferation. We hypothesize that STAT3 GOF signaling in both immune cells and keratinocytes drives pathology in this model, and that non-hematopoietic expression of STAT3 GOF is important in patients with disease given the broad expression pattern of STAT3. Intriguingly, tofacitinib had a modest effect on IMQ-induced disease in WT mice. Thus, targeting of non-immune cells with JAKinibs may be highly relevant to patient therapy. This also emphasizes the unique pathology of STAT3 GOF and highlights the fact that mechanisms of disease in this and other JAK/STAT disorders may not mimic that of more common diseases, such as psoriasis or inflammatory arthritis. Indeed, most STAT3 GOF patients have received multiple therapies and require therapy targeted to their disease mechanism (e.g., JAKinibs and IL-6 blockade) (Forbes et al., 2018; Leiding et al., 2023).

In STAT3 GOF mice treated with tofacitinib, persistence of Th17 in the skin may be due to the fact that IL-6R and IL-23R, both of which are important for Th17 differentiation, rely on JAK1/JAK2/TYK2 (Johnson et al., 2018) and JAK2/TYK2 (Parham et al., 2002), respectively. It is therefore likely that IL-23 signaling still occurs in T cells in the presence of tofacitinib. The IL-22 receptor is expressed mainly on non-hematopoietic cells and signals through JAK1/TYK2, therefore inhibition of this pathway by tofacitinib might explain the reduced epidermal thickness and neutrophil infiltration (Dudakov et al., 2015; Lejeune et al., 2002). HSCT for STAT3 GOF syndrome has yielded mixed results, likely confounded by the fact that transplantation tends to be performed later in disease when patients have significant comorbidities (Leiding et al., 2023). Our finding of incomplete engraftment in BM chimeras, despite receiving the same conditioning in mixed groups, may provide insight into

the relatively low efficacy of HSCT in STAT3 GOF patients. Possible explanations include competitive advantage in the survival of STAT3 GOF hematopoietic cells, altered radiosensitivity due to STAT3 GOF, and/or the inflammatory environment pre-existing in STAT3 GOF mice (Di Maggio et al., 2015; Yu et al., 2009).

STAT3 GOF is a complex monogenic disease that leads to lymphoproliferation and organ-specific autoimmunity in children with a highly variable clinical phenotype. Findings here demonstrate local inflammatory responses mediated by IL-22–producing CD4$^+$ Th17 cells drive skin disease, which is most prominent when STAT3 GOF is also present in skin epithelial cells. While CD8$^+$ T cells have been found to play a role in various disease models, this work emphasizes the importance of examining local immune responses in STAT GOF and other immune dysregulation syndromes and provides new insights into the factors that drive inflammation, which are likely influenced by specific organ and cell type, genetic variables, and environment.

Materials and methods

Mice

All animal study protocols were approved by the Institutional Animal Care and Use Committee at Washington University. All mice were bred and maintained in specific pathogen–free facilities at Washington University. Male and female STAT3 GOF and WT littermates aged 21–22 wk (older adult) or aged 7–9 wk (young adult) were used in all experiments unless stated otherwise. STAT3 GOF (*Stat3*$^{p.G421R/+}$) mice were generated as previously described on a C57BL/6 background (Schmitt et al., 2022). *Stat3*$^{p.T716M/+}$ mice were generated on the C57BL/6 background using CRISPR-Cas9 technology by the Hope Center Transgenic Vectors Core at Washington University School of Medicine (Ran et al., 2013). Mice deficient in IL-22 (*Il22*$^{-/-}$) were generously provided by the laboratory of Dr. Misty Good at the University of North Carolina at Chapel Hill, Chapel Hill, NC, USA (Mihi et al., 2021). *Rag1*$^{-/-}$ (JAX stock #002216), TCRδ-deficient mice (*Tcrd*$^{-/-}$, JAX stock #002120), and IL-17 GFP reporter mice (*Il17*$^{atm1Bcgen/J}$, JAX stock #018472) all on the C57BL/6 background were purchased from Jackson Laboratories. C57BL/6 congenic for the Ly5.1 marker (B6.SJL-*Ptprc*^{a}*Pepc*^{b}/BoyCrCrl, strain #564) was purchased from Charles River.

Generation of Stat3$^{p.T716M/+}$ mice

CRISPR guide RNAs (gRNAs) for in vitro testing were identified and cloned into BbsI digested plasmid pX330 (# 42230; Addgene, gRNA sequence: 5′-GGTCATTCTGTAGGAAAGGG-3′). Single-guide RNA (sgRNA) activity was validated in vitro by transfection of NIH3T3 cells using ROCHE Xtremegene HP. Cell pools were harvested 48 h later for genomic DNA prep, followed by Sanger sequencing of PCR products spanning the gRNA/Cas9 cleavage site and TIDE analysis (https://tide.nki.nl/) of sequence trace files. T7 sgRNA template was PCR amplified, gel-purified, and in vitro transcribed with the MEGAshortscript T7 kit (Life Technologies). T7 Cas9 template was PCR amplified, gel purified, and in vitro transcribed with the T7 mMessage mMachine Ultra kit (Life technologies). After transcription, RNA was purified with Megaclear kit (Life Technologies). A single-stranded oligodeoxynucleotide (ssODN donor) DNA with the mutation centered within the oligo was ordered from IDT as an ultramer oligo. Injection concentrations were 50 ng/µl Cas9, 25 ng/µl gRNA, and 20 ng/µl ssODN. ssODN sequence: 5′-CCCCCTCCA TTGTGTCTTGTCAACCTGGCCCTTCCCACTCCTGCCGTCCCC CCTTTCCTACAGAATGACCTGCAGCAATACCATTGACCTGCC GATGTCCCCCCGCACTTTAGATTCATTGATGCAGTTTGGAAA TAACGGTGAAGGTGCTGAGCCCTCAGCAG-3′. Founders were identified using Qiagen Pyrosequencer and Pyromark Q96 2.5.7 software. One-cell fertilized embryos were injected into the pronucleus and cytoplasm of each zygote. Microinjections and mouse transgenesis experiments were performed as described previously (Pease and Saunders, 2011; Behringer et al., 2014).

Mice were screened using a single-nucleotide polymorphism (SNP) assay with primer/probe sets from ABI/Life Technologies and TaqMan Genotyping Master Mix (Cat#4371355; Thermo Fisher Scientific). Forward primer: 5′-CCTCCATTGTGTCTTGTC AACCT-3′, reverse primer: 5′-CACCGTTATTTCCAAACTGCA TCAA-3′, Reporter 1: 5′-CTGCAGGTCGTTCTGT-3′ (VIC, WT sequence), and Reporter 2: 5′-TGCAGGTCATTCTGT-3′ (fluorescein amidite, SNP sequence).

In vitro Th17 polarization

CD4$^+$ T cells were enriched from the spleen and lymph nodes using the MojoSort Mouse CD4 T cell Isolation Kit (BioLegend). Naïve CD4$^+$ T cells (CD3e$^+$ CD25$^-$ CD4$^+$ CD44$^-$ CD62L$^+$) were sorted on a BD FACS AriaFusion flow cytometer (BD Biosciences). 2 × 10^5 sorted cells were cultured for 4 days on a 96-well flat-bottom plate at 37°C in complete RPMI 1640 medium supplemented with 10% FBS, 1% penicillin/streptomycin, and 50 µM β-mercaptoethanol. Cells were stimulated with 10 µg/ml plate-bound anti-CD3 (clone 145-2C11; BioXCell) and 2 µg/ml anti-CD28 (clone 37.51; BioXCell). For Th17 polarization, the culture medium included 5 ng/ml rmTGF-β1 (Cell Signaling Technology), 10 µg/ml anti-IFNγ (clone: XMG1.2; BioXCell), 10 µg/ml anti-IL-4 (clone: 11B11; BioXCell), with or without rmIL-6 (Peprotech).

IMQ-induced skin inflammation model

To induce psoriasiform dermatitis in mice, 5% IMQ cream (Taro) was applied to the dorsal and ventral sides of both ears for 7 consecutive days. Mice received ∼5 mg IMQ daily. Ear thickness was measured daily with a 0.01-mm dial thickness gauge (Peacock) by a single-blinded scorer, calculated by the average of three separate measurements of the right ear. Mice were analyzed on day 7 of IMQ treatment.

Antibody depletion

For CD8 depletion experiments, mice were treated with 150 µg anti-CD8a (clone: 53-6.7; BioXCell) intraperitoneally for 7 consecutive days, starting 24 h prior to the first IMQ treatment. CD8 T cell depletion was verified by flow cytometry. For IL-17A depletion experiments, mice were treated with 250 µg anti-IL-17A (BioXCell) intraperitoneally 2 days prior to the first IMQ treatment and then on day 4 after the first IMQ treatment.

Histology

For histological analysis of the mouse skin, ears were isolated at time of sacrifice and preserved overnight in 4% paraformaldehyde prior to paraffin embedding and H&E staining (Digestive Diseases Research Cores Center, Washington University School of Medicine or Nationwide Histology). Whole slides were imaged with an Olympus BX61VS slide scanner microscope. Average epidermal thickness, blood vessel area, and cellular infiltrate count were measured from three representative areas of each slide by a single-blinded scorer using Qupath-0.3.1 software (Bankhead et al., 2017). Pathological score was determined by calculating the sum of the average epidermal thickness/10 + average blood vessel area/1,000 + average cellular infiltrate count/100. Images processed with ImageJ (Schneider et al., 2012).

Skin tissue processing for flow cytometry

Dorsal and ventral halves of ears were separated, minced, and placed in 1.5 ml RPMI 1640 (Corning) supplemented with 1% antibiotic-antimycotic (Corning), 1% MEM nonessential amino acids (Corning), 1 mM sodium pyruvate (Corning), 25 mM HEPES Buffer (Corning), 50 µM β-mercaptoethanol. Ear tissue was then digested with 125 µg/ml LiberaseTL (Roche) and 100 µg/ml DNase I (Roche) on a rotating shaker for 90 min. Tissue was gently homogenized by passing through a syringe, then filtered through a 70-µm cell strainer to obtain single cell suspensions for flow cytometry.

Flow cytometry

Cells from the skin, CLN, and whole blood were isolated and stained as indicated. For surface staining, cells were washed with cell staining buffer (1X Dulbecco's phosphate-buffered saline [Corning] + 2% FBS + 1 mM EDTA), treated with Fc block (clone 2.4G2), stained with surface antibodies for 30 min at 4°C, then washed again with cell staining buffer. For intranuclear staining, cells were fixed for 1 h at room temperature with the eBioscience Foxp3/Transcription Factor Staining Buffer kit and washed with permeabilization buffer (Thermo Fisher Scientific). Cells were stained with intranuclear antibodies for 1 h at room temperature and then washed with cell staining buffer. For intracellular staining, cells were stimulated with 5 ng/ml PMA (Sigma-Aldrich) and 0.5 µM ionomycin (Sigma-Aldrich) with GolgiPlug (BD) for 4 h at 37°C + 5% CO_2 prior to surface staining. Cells were fixed and permeabilized with the BD Cytofix/Cytoperm solution (BD Biosciences), washed with permeabilization buffer (Thermo Fisher Scientific), and then stained for intracellular antibodies for 30 min at 4°C. Dead cells were distinguished by Zombie Yellow (BioLegend). For GFP expression analysis, unstimulated cells were prefixed with 1% paraformaldehyde at 37°C for 10 min before proceeding to fixation and permeabilization. Flow cytometry was performed on an LSRFortessa (BD Biosciences) or Cytek Aurora, and data were analyzed using FlowJo 10.7.1. The following fluorochrome-conjugated antibodies were used: anti-mouse CD3ε (145-2C11; BioLegend), anti-mouse CD62L (MEL-14; BioLegend), anti-mouse IL-22 (Poly5164; BioLegend), anti-mouse/human CD44 (IM7; BioLegend), anti-mouse FOXP3 (FJK-16s; Invitrogen), anti-mouse CD4 (GK1.5; BioLegend), anti-mouse CD45.2 (104; BD Biosciences), anti-mouse CD19 (6D5; BioLegend), anti-mouse CD8a (53-6.7; BD Biosciences), anti-mouse NK-1.1 (PK136; BioLegend), anti-mouse CD64 (X54-5/7.1; BioLegend), anti-mouse RORγt (Q31-378; BD Biosciences), anti-mouse IL-17A (TC11-18H10; BD Biosciences), anti-mouse/human CD11b (M1-70; BioLegend), anti-mouse CD11c (HL3; BD Biosciences), anti-mouse I-Ab (AF6-120.1; BioLegend), anti-mouse IFNγ (XMG1.2; BD Biosciences), anti-mouse γδ TCR (GL3; BD Biosciences), anti-mouse Ly-6G (1A8; BioLegend), anti-mouse CD196 (29-2L17; BioLegend), anti-mouse CD24 (M1/69; BD Biosciences), anti-mouse CD25 (PC61; BD Biosciences), anti-mouse IL-4 (11B11; BD Biosciences), anti-mouse GATA3 (L50-823; BD Biosciences), and anti-mouse T-Bet (4B10; BD Biosciences).

BM chimeras

BM chimeras were generated by transplanting whole BM cells from 7- to 12-wk-old CD45.2$^+$ donors into CD45.1$^+$ recipients that were randomly housed together and lethally irradiated with 2 doses of 550 cGy. 2×10^6 cells were injected retro-orbitally into lethally irradiated recipients. Recipients received 0.5 mg/ml sulfamethoxazole and 0.1 mg/ml trimethoprim in drinking water ad libitum for 2 wk after transplant. Engraftment was assessed in the peripheral blood at 6, 8, 10, and 12 wk after transplant. IMQ experiments were started 12 wk after the transplant.

scRNA-seq and TCR-seq

Bulk T cells were isolated from the CLN of two untreated and two IMQ-treated WT and STAT3 GOF littermates (one male and one female per group; eight separate groups/mice) using the EasySep Mouse T cell Isolation Kit (StemCell) following the manufacturer's instructions. 1×10^6 purified T cells were labeled with anti-mouse CD3e (C0182), TCRβ (C0120), CD4 (C0001), CD8a (C0002), CD44 (C0073), and CD62L (C0112) Totalseq-C antibodies (BioLegend) for CITE-seq (Stoeckius et al., 2017). The 5′ GEX v2 libraries were generated and dual-indexed with VDJ and surface immune receptor sequencing following the manufacturer's instructions, loading 30,000 cells per well (10X Genomics). Libraries were sequenced and processed by the Genome Technology Access Center at the McDonnell Genome Institute at Washington University School of Medicine following the manufacturer's instructions (10X Genomics). Raw data were filtered, aligned, and aggregated using Cellranger v.6.0.0, and feature-barcode matrix analysis was performed in Rstudio with the Seurat v4 R package (Hao et al., 2021). A total of 135,825 cells were filtered based on mitochondrial content and feature count. Cells with >20% mitochondrial DNA were filtered from analysis, leaving a total of 135,567 cells. Normalization, scaling, and dimensionality reduction were performed using default parameters, with resolution at 0.8 and 30 dimensions for the reduction. For CITE-seq, RNA and protein data were integrated using weighted nearest-neighbor analysis (Hao et al., 2021). The CellSelector function was used to separate single-positive CD4 and CD8 populations based on surface protein expression, and the CD4 and CD8 populations were renormalized using the same procedure. Non-T cell contaminants were removed from

analysis. Clusters were manually annotated based on CD44 and CD62L surface protein expression and by expression of canonical genes found in literature. Differential gene expression was calculated using the "FindMarkers" function and the default Wilcoxon rank-sum test. Seurat (Hao et al., 2021), ggVolcanoR (Mullan et al., 2021), ggplot2 (Wickham, 2016), and dittoseq (Bunis et al., 2021) R packages were used for data visualization. T cell clonotypes were assigned and clonotype dynamics were analyzed using the ScRepertoire R package (Borcherding et al., 2020). Clonotypes were assigned using the "cloneCall = strict" function, which integrates the VDJC genes of the TCR and the nucleotide sequence of the CDR3 region to define clonotype.

Adoptive transfer

IL-17-GFP reporter mice and STAT3 GOF × IL-17-GFP mice were treated with IMQ for 7 consecutive days. CLN and spleen were isolated and $CD4^+$ T cells were purified using the MojoSort Mouse CD4 T cell Negative Isolation Kit (BioLegend). Purified $CD4^+$ T cells were >95% pure by flow cytometry. 5×10^6 cells were injected into the tail veins of sex-matched *Rag1*$^{-/-}$ mice. 24 h after transfer, *Rag1*$^{-/-}$ recipients were treated with IMQ for 7 consecutive days.

Oral tofacitinib treatment

Tofacitinib citrate (MedChemExpress) was delivered in chow formulation by combining Nutra-gel dry mix kit (Bio-serv) with tofacitinib at a ratio of 1 g tofacitinib to 1 kg Nutra-gel. Briefly, Nutra-gel was prepared according to the manufacturer's instructions (Senkevitch et al., 2018). Tofacitinib powder was added to the heated water and dry powder mixture and then mixed in a blender for 20–30 s. Nutra-gel with and without tofacitinib was stored at 4°C until use for up to 7 days. Mice were given Nutra-gel chow without drug for 3 days to acclimate to the diet before starting tofacitinib treatment. Mice received fresh Nutra-gel daily (with or without tofacitinib) with ad libitum access.

Quantification and statistical analysis

Prism 9 was used to calculate all statistics, the details of which can be found in the figure legends. A two-tailed unpaired *t* test or Welch's *t* test was used for comparisons of two. For comparisons of four groups, samples were analyzed by one-way ANOVA with Sidak's multiple comparison test. Percent change in ear thickness was analyzed by two-way repeated measures ANOVA with Sidak's multiple comparisons test. For comparisons of three or more groups with two independent variables, two-way ANOVA with Sidak's multiple comparisons test was used. *P < 0.05, **P < 0.01, ***P < 0.001, ****P < 0.0001.

Online supplemental material

Fig. S1 shows quantified cell populations in older adult WT and STAT3 GOF (*Stat3*$^{p.G421R/+}$) mice. Fig. S2 shows quantified cell populations in skin and CLN of IMQ-treated young adult WT and STAT3 GOF mice. Fig. S3 shows $CD4^+$ T cells are sufficient, and γδ T cells and $CD8^+$ T cells are not required to mediate IMQ-induced inflammation in STAT3 GOF mice. Fig. S4 shows STAT3 GOF BM can exacerbate inflammation in WT mice. Fig. S5 shows analysis of STAT3 GOF CD8 T cells by scRNA-seq.

Data availability

The data in the figures are available in the published article and its online supplemental material. The scRNA-seq data in Figs. 5 and 6 have been deposited under accession no. GSE240205. Further information and requests for resources and reagents should be directed to and will be fulfilled by the lead contact, Megan A. Cooper (cooper_m@wustl.edu).

Acknowledgments

The graphical abstract was generated with https://Biorender.com.

This work was supported by National Institutes of Health/National Institute of Allergy and Infectious Diseases (NIH/NIAID) 1P01AI155393 (M.A. Cooper), the Washington University Rheumatic Diseases Research Resource-Based Center P30AR073752 (M.A. Cooper and E.G. Schmitt), NIH K12HD076224 (E.G. Schmitt), National Institute of Biomedical Imaging and Bioengineering T32 EB028092 (K.A. Toth), Washington University Digestive Diseases Research Core Center P30DK052574 (Advanced Imaging and Tissue Analysis Core), the Scleroderma Foundation (M.A. Cooper), the Children's Discovery Institute at St. Louis Children's Hospital (M.A. Cooper), and the Hope Center Transgenic Vectors Core at Washington University School of Medicine. We thank the Genome Technology Access Center at the McDonnell Genome Institute at Washington University School of Medicine for help with genomic analysis. The Center is partially supported by National Cancer Institute Cancer Center Support Grant #P30 CA91842 to the Siteman Cancer Center from the National Center for Research Resources (NCRR), a component of the NIH, and NIH Roadmap for Medical Research. This work was supported in part by the Division of Intramural Research of the NIAID, NIH (to M.S. Lionakis). This publication is solely the responsibility of the authors and does not necessarily represent the official view of NCRR or NIH.

Author contributions: K.A. Toth: Conceptualization, Data curation, Formal analysis, Investigation, Methodology, Project administration, Validation, Visualization, Writing - original draft, Writing - review & editing, E.G. Schmitt: Conceptualization, Writing - review & editing, A. Kolicheski: Data curation, Formal analysis, Resources, Visualization, Writing - review & editing, Z.J. Greenberg: Investigation, E. Levendosky: Investigation, Resources, N. Saucier: Data curation, Resources, K. Trammel: Investigation, Resources, V. Oikonomou: Investigation, M.S. Lionakis: Resources, Writing - review & editing, E. Klechevsky: Investigation, Resources, Writing - review & editing, B.S. Kim: Conceptualization, Writing - review & editing, L.G. Schuettpelz: Investigation, N. Saligrama: Supervision, M.A. Cooper: Conceptualization, Funding acquisition, Methodology, Project administration, Supervision, Writing - original draft, Writing - review & editing.

Disclosures: B.S. Kim is founder of Klirna Biotech; he has served as a consultant for 23andMe, ABRAX Japan, AbbVie, Almirall, Amagma Therapeutics, Amgen, Arcutis Biotherapeutics, Arena Pharmaceuticals, argenx, AstraZeneca, Boehringer Ingelheim,

Bristol Myers Squibb, Cara Therapeutics, Clexio Biosciences, Eli Lilly and Company, Escient Pharmaceuticals, Evommune, Galderma, Genentech, GlaxoSmithKline, Granular Therapeutics, Incyte Corporation, Innovaderm Research, Janssen, Kiniksa, LEO Pharma, Maruho, Novartis, Pfizer, Recens Medical, Regeneron Pharmaceuticals, Sanofi, Septerna, Vial, WebMD; he has stock in ABRAX Japan, KliRNA Biotech, Locus Biosciences, and Recens Medical; he holds a patent for the use of JAK1 inhibitors for chronic pruritus; he has a patent pending for the use of JAK inhibitors for interstitial cystitis. He has research grants from AbbVie, Cara Therapeutics, LEO Pharma, and Veradermics. No other disclosures were reported.

Submitted: 14 November 2023
Revised: 29 April 2024
Accepted: 21 May 2024

References

Al-Ismaeel, Q., C.P. Neal, H. Al-Mahmoodi, Z. Almutairi, I. Al-Shamarti, K. Straatman, N. Jaunbocus, A. Irvine, E. Issa, C. Moreman, et al. 2019. ZEB1 and IL-6/11-STAT3 signalling cooperate to define invasive potential of pancreatic cancer cells via differential regulation of the expression of S100 proteins. *Br. J. Cancer*. 121:65–75. https://doi.org/10.1038/s41416-019-0483-9

Bankhead, P., M.B. Loughrey, J.A. Fernández, Y. Dombrowski, D.G. McArt, P.D. Dunne, S. McQuaid, R.T. Gray, L.J. Murray, H.G. Coleman, et al. 2017. QuPath: Open source software for digital pathology image analysis. *Sci. Rep.* 7:16878. https://doi.org/10.1038/s41598-017-17204-5

Barnes, J.L., M.W. Plank, K. Asquith, S. Maltby, L.R. Sabino, G.E. Kaiko, A. Lochrin, J.C. Horvat, J.R. Mayall, R.Y. Kim, et al. 2021. T-helper 22 cells develop as a distinct lineage from Th17 cells during bacterial infection and phenotypic stability is regulated by T-bet. *Mucosal Immunol.* 14: 1077–1087. https://doi.org/10.1038/s41385-021-00414-6

Borcherding, N., N.L. Bormann, and G. Kraus. 2020. scRepertoire: An R-based toolkit for single-cell immune receptor analysis. *F1000 Res.* 9:47. https://doi.org/10.12688/f1000research.22139.1

Bovenschen, H.J., P.C. van de Kerkhof, P.E. van Erp, R. Woestenenk, I. Joosten, and H.J. Koenen. 2011. Foxp3$^+$ regulatory T cells of psoriasis patients easily differentiate into IL-17A-producing cells and are found in lesional skin. *J. Invest. Dermatol.* 131:1853–1860. https://doi.org/10.1038/jid.2011.139

Bunis, D.G., J. Andrews, G.K. Fragiadakis, T.D. Burt, and M. Sirota. 2021. dittoSeq: universal user-friendly single-cell and bulk RNA sequencing visualization toolkit. *Bioinformatics*. 36:5535–5536. https://doi.org/10.1093/bioinformatics/btaa1011

Cai, Y., X. Shen, C. Ding, C. Qi, K. Li, X. Li, V.R. Jala, H.G. Zhang, T. Wang, J. Zheng, and J. Yan. 2011. Pivotal role of dermal IL-17-producing γδ T cells in skin inflammation. *Immunity*. 35:596–610. https://doi.org/10.1016/j.immuni.2011.08.001

Di Maggio, F.M., L. Minafra, G.I. Forte, F.P. Cammarata, D. Lio, C. Messa, M.C. Gilardi, and V. Bravatà. 2015. Portrait of inflammatory response to ionizing radiation treatment. *J. Inflamm.* 12:14. https://doi.org/10.1186/s12950-015-0058-3

Dudakov, J.A., A.M. Hanash, and M.R. van den Brink. 2015. Interleukin-22: Immunobiology and pathology. *Annu. Rev. Immunol.* 33:747–785. https://doi.org/10.1146/annurev-immunol-032414-112123

Eyerich, K., V. Dimartino, and A. Cavani. 2017. IL-17 and IL-22 in immunity: Driving protection and pathology. *Eur. J. Immunol.* 47:607–614. https://doi.org/10.1002/eji.201646723

Flanagan, S.E., E. Haapaniemi, M.A. Russell, R. Caswell, H.L. Allen, E. De Franco, T.J. McDonald, H. Rajala, A. Ramelius, J. Barton, et al. 2014. Activating germline mutations in STAT3 cause early-onset multi-organ autoimmune disease. *Nat. Genet.* 46:812–814. https://doi.org/10.1038/ng.3040

Flutter, B., and F.O. Nestle. 2013. TLRs to cytokines: Mechanistic insights from the imiquimod mouse model of psoriasis. *Eur. J. Immunol.* 43: 3138–3146. https://doi.org/10.1002/eji.201343801

Forbes, L.R., T.P. Vogel, M.A. Cooper, J. Castro-Wagner, E. Schussler, K.G. Weinacht, A.S. Plant, H.C. Su, E.J. Allenspach, M. Slatter, et al. 2018. Jakinibs for the treatment of immune dysregulation in patients with gain-of-function signal transducer and activator of transcription 1 (STAT1) or STAT3 mutations. *J. Allergy Clin. Immunol.* 142:1665–1669. https://doi.org/10.1016/j.jaci.2018.07.020

Gaffen, S.L., R. Jain, A.V. Garg, and D.J. Cua. 2014. The IL-23-IL-17 immune axis: From mechanisms to therapeutic testing. *Nat. Rev. Immunol.* 14: 585–600. https://doi.org/10.1038/nri3707

Gharibi, T., Z. Babaloo, A. Hosseini, M. Abdollahpour-Alitappeh, V. Hashemi, F. Marofi, K. Nejati, and B. Baradaran. 2020. Targeting STAT3 in cancer and autoimmune diseases. *Eur. J. Pharmacol.* 878:173107. https://doi.org/10.1016/j.ejphar.2020.173107

Guo, X., J. Qiu, T. Tu, X. Yang, L. Deng, R.A. Anders, L. Zhou, and Y.X. Fu. 2014. Induction of innate lymphoid cell-derived interleukin-22 by the transcription factor STAT3 mediates protection against intestinal infection. *Immunity*. 40:25–39. https://doi.org/10.1016/j.immuni.2013.10.021

Haapaniemi, E.M., M. Kaustio, H.L. Rajala, A.J. van Adrichem, L. Kainulainen, V. Glumoff, R. Doffinger, H. Kuusanmäki, T. Heiskanen-Kosma, L. Trotta, et al. 2015. Autoimmunity, hypogammaglobulinemia, lymphoproliferation, and mycobacterial disease in patients with activating mutations in STAT3. *Blood*. 125:639–648. https://doi.org/10.1182/blood-2014-04-570101

Hao, Y., S. Hao, E. Andersen-Nissen, W.M. Mauck III, S. Zheng, A. Butler, M.J. Lee, A.J. Wilk, C. Darby, M. Zager, et al. 2021. Integrated analysis of multimodal single-cell data. *Cell*. 184:3573–3587.e29. https://doi.org/10.1016/j.cell.2021.04.048

Harper, E.G., C. Guo, H. Rizzo, J.V. Lillis, S.E. Kurtz, I. Skorcheva, D. Purdy, E. Fitch, M. Iordanov, and A. Blauvelt. 2009. Th17 cytokines stimulate CCL20 expression in keratinocytes in vitro and in vivo: Implications for psoriasis pathogenesis. *J. Invest. Dermatol.* 129:2175–2183. https://doi.org/10.1038/jid.2009.65

Hillmer, E.J., H. Zhang, H.S. Li, and S.S. Watowich. 2016. STAT3 signaling in immunity. *Cytokine Growth Factor Rev.* 31:1–15. https://doi.org/10.1016/j.cytogfr.2016.05.001

Johnson, D.E., R.A. O'Keefe, and J.R. Grandis. 2018. Targeting the IL-6/JAK/STAT3 signalling axis in cancer. *Nat. Rev. Clin. Oncol.* 15:234–248. https://doi.org/10.1038/nrclinonc.2018.8

Kane, A., E.K. Deenick, C.S. Ma, M.C. Cook, G. Uzel, and S.G. Tangye. 2014. STAT3 is a central regulator of lymphocyte differentiation and function. *Curr. Opin. Immunol.* 28:49–57. https://doi.org/10.1016/j.coi.2014.01.015

Khoury, T., V. Molho-Pessach, Y. Ramot, A.R. Ayman, O. Elpeleg, N. Berkman, A. Zlotogorski, and Y. Ilan. 2017. Tocilizumab promotes regulatory T-cell alleviation in STAT3 gain-of-function-associated multi-organ autoimmune syndrome. *Clin. Ther.* 39:444–449. https://doi.org/10.1016/j.clinthera.2017.01.004

Kitagawa, Y., N. Ohkura, Y. Kidani, A. Vandenbon, K. Hirota, R. Kawakami, K. Yasuda, D. Motooka, S. Nakamura, M. Kondo, et al. 2017. Guidance of regulatory T cell development by Satb1-dependent super-enhancer establishment. *Nat. Immunol.* 18:173–183. https://doi.org/10.1038/ni.3646

Leiding, J.W., T.P. Vogel, V.G.J. Santarlas, R. Mhaskar, M.R. Smith, A. Carisey, A. Vargas-Hernández, M. Silva-Carmona, M. Heeg, A. Rensing-Ehl, et al. 2023. Monogenic early-onset lymphoproliferation and autoimmunity: Natural history of STAT3 gain-of-function syndrome. *J. Allergy Clin. Immunol.* 151:1081–1095. https://doi.org/10.1016/j.jaci.2022.09.002

Lejeune, D., L. Dumoutier, S. Constantinescu, W. Kruijer, J.J. Schuringa, and J.C. Renauld. 2002. Interleukin-22 (IL-22) activates the JAK/STAT, ERK, JNK, and p38 MAP kinase pathways in a rat hepatoma cell line. Pathways that are shared with and distinct from IL-10. *J. Biol. Chem.* 277: 33676–33682. https://doi.org/10.1074/jbc.M204204200

Levy, D.E., and C.K. Lee. 2002. What does Stat3 do? *J. Clin. Invest.* 109: 1143–1148. https://doi.org/10.1172/JCI0215650

Liang, S.C., X.Y. Tan, D.P. Luxenberg, R. Karim, K. Dunussi-Joannopoulos, M. Collins, and L.A. Fouser. 2006. Interleukin (IL)-22 and IL-17 are coexpressed by Th17 cells and cooperatively enhance expression of antimicrobial peptides. *J. Exp. Med.* 203:2271–2279. https://doi.org/10.1084/jem.20061308

Masle-Farquhar, E., K.J.L. Jackson, T.J. Peters, G. Al-Eryani, M. Singh, K.J. Payne, G. Rao, D.T. Avery, G. Apps, J. Kingham, et al. 2022. STAT3 gain-of-function mutations connect leukemia with autoimmune disease by pathological NKG2D^{hi} CD8$^+$ T cell dysregulation and accumulation. *Immunity*. 55:2386–2404.e8. https://doi.org/10.1016/j.immuni.2022.11.001

Mihi, B., Q. Gong, L.S. Nolan, S.E. Gale, M. Goree, E. Hu, W.E. Lanik, J.M. Rimer, V. Liu, O.B. Parks, et al. 2021. Interleukin-22 signaling

attenuates necrotizing enterocolitis by promoting epithelial cell regeneration. *Cell Rep. Med.* 2:100320. https://doi.org/10.1016/j.xcrm.2021.100320

Milner, J.D., T.P. Vogel, L. Forbes, C.A. Ma, A. Stray-Pedersen, J.E. Niemela, J.J. Lyons, K.R. Engelhardt, Y. Zhang, N. Topcagic, et al. 2015. Early-onset lymphoproliferation and autoimmunity caused by germline STAT3 gain-of-function mutations. *Blood.* 125:591–599. https://doi.org/10.1182/blood-2014-09-602763

Miyoshi, K., M. Takaishi, K. Nakajima, M. Ikeda, T. Kanda, M. Tarutani, T. Iiyama, N. Asao, J. DiGiovanni, and S. Sano. 2011. Stat3 as a therapeutic target for the treatment of psoriasis: A clinical feasibility study with STA-21, a Stat3 inhibitor. *J. Invest. Dermatol.* 131:108–117. https://doi.org/10.1038/jid.2010.255

Moos, S., A.N. Mohebiany, A. Waisman, and F.C. Kurschus. 2019. Imiquimod-induced psoriasis in mice depends on the IL-17 signaling of keratinocytes. *J. Invest. Dermatol.* 139:1110–1117. https://doi.org/10.1016/j.jid.2019.01.006

Mullan, K.A., L.M. Bramberger, P.R. Munday, G. Goncalves, J. Revote, N.A. Mifsud, P.T. Illing, A. Anderson, P. Kwan, A.W. Purcell, and C. Li. 2021. ggVolcanoR: A Shiny app for customizable visualization of differential expression datasets. *Comput. Struct. Biotechnol. J.* 19:5735–5740. https://doi.org/10.1016/j.csbj.2021.10.020

O'Shea, J.J., M. Gadina, and R.D. Schreiber. 2002. Cytokine signaling in 2002: New surprises in the jak/stat pathway. *Cell.* 109:S121–S131. https://doi.org/10.1016/S0092-8674(02)00701-8

O'Shea, J.J., and R. Plenge. 2012. JAK and STAT signaling molecules in immunoregulation and immune-mediated disease. *Immunity.* 36:542–550. https://doi.org/10.1016/j.immuni.2012.03.014

O'Shea, J.J., D.M. Schwartz, A.V. Villarino, M. Gadina, I.B. McInnes, and A. Laurence. 2015. The JAK-STAT pathway: Impact on human disease and therapeutic intervention. *Annu. Rev. Med.* 66:311–328. https://doi.org/10.1146/annurev-med-051113-024537

Parham, C., M. Chirica, J. Timans, E. Vaisberg, M. Travis, J. Cheung, S. Pflanz, R. Zhang, K.P. Singh, F. Vega, et al. 2002. A receptor for the heterodimeric cytokine IL-23 is composed of IL-12Rbeta1 and a novel cytokine receptor subunit, IL-23R. *J. Immunol.* 168:5699–5708. https://doi.org/10.4049/jimmunol.168.11.5699

Pease, S.,and T.L. Saunders, editors. 2011. Advanced Protocols for Animal Transgenesis. Vol. 21. Springer Berlin Heidelberg, Berlin, Heidelberg. https://doi.org/10.1007/978-3-642-20792-1

Ran, F.A., P.D. Hsu, J. Wright, V. Agarwala, D.A. Scott, and F. Zhang. 2013. Genome engineering using the CRISPR-Cas9 system. *Nat. Protoc.* 8:2281–2308. https://doi.org/10.1038/nprot.2013.143

Ravipati, A., S. Nolan, M. Alphonse, D. Dikeman, C. Youn, Y. Wang, N. Orlando, G. Patrick, S. Lee, R.V. Ortines, et al. 2022. IL-6R/Signal transducer and activator of transcription 3 signaling in keratinocytes rather than in T cells induces psoriasis-like dermatitis in mice. *J. Invest. Dermatol.* 142:1126–1135.e4. https://doi.org/10.1016/j.jid.2021.09.012

Behringer, R., M. Gertsenstein, K. Vintersten Nagy, and A. Nagy. 2014. Manipulating the Mouse Embryo: A Laboratory Manual. Fourth edition. Cold Spring Harbor Laboratory Press, Cold Spring Harbor, New York, NY.

Sano, S., K.S. Chan, S. Carbajal, J. Clifford, M. Peavey, K. Kiguchi, S. Itami, B.J. Nickoloff, and J. DiGiovanni. 2005. Stat3 links activated keratinocytes and immunocytes required for development of psoriasis in a novel transgenic mouse model. *Nat. Med.* 11:43–49. https://doi.org/10.1038/nm1162

Schmitt, E.G., K.A. Toth, S.I. Risma, A. Kolicheski, N. Saucier, R.J.F. Berrios, Z.J. Greenberg, J.W. Leiding, J.J. Bleesing, A. Thatayatikom, et al. 2022. A human STAT3 gain-of-function variant confers T cell dysregulation without predominant Treg dysfunction in mice. *JCI Insight* 7:e162695. https://doi.org/10.1172/jci.insight.162695

Schneider, C.A., W.S. Rasband, and K.W. Eliceiri. 2012. NIH image to ImageJ: 25 years of image analysis. *Nat. Methods.* 9:671–675. https://doi.org/10.1038/nmeth.2089

Senkevitch, E., W. Li, J.A. Hixon, C. Andrews, S.D. Cramer, G.T. Pauly, T. Back, K. Czarra, and S.K. Durum. 2018. Inhibiting Janus Kinase 1 and BCL-2 to treat T cell acute lymphoblastic leukemia with IL7-Rα mutations. *Oncotarget.* 9:22605–22617. https://doi.org/10.18632/oncotarget.25194

Shi, Y., Z. Chen, Z. Zhao, Y. Yu, H. Fan, X. Xu, X. Bu, and J. Gu. 2019. IL-21 induces an imbalance of Th17/Treg cells in moderate-to-severe plaque psoriasis patients. *Front. Immunol.* 10:1865. https://doi.org/10.3389/fimmu.2019.01865

Silva-Carmona, M., T.P. Vogel, S. Marchal, M. Guesmi, J.C. Dubus, S. Leroy, A. Fabre, V. Barlogis, L.R. Forbes, and L. Giovannini-Chami. 2020. Successful treatment of interstitial lung disease in STAT3 gain-of-function using JAK inhibitors. *Am. J. Respir. Crit. Care Med.* 202:893–897. https://doi.org/10.1164/rccm.201906-1204LE

Stoeckius, M., C. Hafemeister, W. Stephenson, B. Houck-Loomis, P.K. Chattopadhyay, H. Swerdlow, R. Satija, and P. Smibert. 2017. Simultaneous epitope and transcriptome measurement in single cells. *Nat. Methods.* 14:865–868. https://doi.org/10.1038/nmeth.4380

Sumaria, N., B. Roediger, L.G. Ng, J. Qin, R. Pinto, L.L. Cavanagh, E. Shklovskaya, B. Fazekas de St Groth, J.A. Triccas, and W. Weninger. 2011. Cutaneous immunosurveillance by self-renewing dermal gammadelta T cells. *J. Exp. Med.* 208:505–518. https://doi.org/10.1084/jem.20101824

Sutton, C.E., S.J. Lalor, C.M. Sweeney, C.F. Brereton, E.C. Lavelle, and K.H. Mills. 2009. Interleukin-1 and IL-23 induce innate IL-17 production from gammadelta T cells, amplifying Th17 responses and autoimmunity. *Immunity.* 31:331–341. https://doi.org/10.1016/j.immuni.2009.08.001

Suzuki, H., B. Wang, G.M. Shivji, P. Toto, P. Amerio, M.A. Tomai, R.L. Miller, and D.N. Sauder. 2000. Imiquimod, a topical immune response modifier, induces migration of Langerhans cells. *J. Invest. Dermatol.* 114:135–141. https://doi.org/10.1046/j.1523-1747.2000.00833.x

Tortola, L., E. Rosenwald, B. Abel, H. Blumberg, M. Schäfer, A.J. Coyle, J.C. Renauld, S. Werner, J. Kisielow, and M. Kopf. 2012. Psoriasiform dermatitis is driven by IL-36-mediated DC-keratinocyte crosstalk. *J. Clin. Invest.* 122:3965–3976. https://doi.org/10.1172/JCI63451

Toth, K.A., E.G. Schmitt, and M.A. Cooper. 2023. Deficiencies and dysregulation of STAT pathways that drive inborn errors of immunity: Lessons from patients and mouse models of disease. *J. Immunol.* 210:1463–1472. https://doi.org/10.4049/jimmunol.2200905

Ueno, A., H. Jijon, R. Chan, K. Ford, C. Hirota, G.G. Kaplan, P.L. Beck, M. Iacucci, M. Fort Gasia, H.W. Barkema, et al. 2013. Increased prevalence of circulating novel IL-17 secreting Foxp3 expressing $CD4^+$ T cells and defective suppressive function of circulating $Foxp3^+$ regulatory cells support plasticity between Th17 and regulatory T cells in inflammatory bowel disease patients. *Inflamm. Bowel Dis.* 19:2522–2534. https://doi.org/10.1097/MIB.0b013e3182a85709

Van Belle, A.B., M. de Heusch, M.M. Lemaire, E. Hendrickx, G. Warnier, K. Dunussi-Joannopoulos, L.A. Fouser, J.C. Renauld, and L. Dumoutier. 2012. IL-22 is required for imiquimod-induced psoriasiform skin inflammation in mice. *J. Immunol.* 188:462–469. https://doi.org/10.4049/jimmunol.1102224

van der Fits, L., S. Mourits, J.S. Voerman, M. Kant, L. Boon, J.D. Laman, F. Cornelissen, A.M. Mus, E. Florencia, E.P. Prens, and E. Lubberts. 2009. Imiquimod-induced psoriasis-like skin inflammation in mice is mediated via the IL-23/IL-17 axis. *J. Immunol.* 182:5836–5845. https://doi.org/10.4049/jimmunol.0802999

Vogel, T.P., J.W. Leiding, M.A. Cooper, and L.R. Forbes Satter. 2023. STAT3 gain-of-function syndrome. *Front. Pediatr.* 10:770077. https://doi.org/10.3389/fped.2022.770077

Vogel, T.P., J.D. Milner, and M.A. Cooper. 2015. The ying and yang of STAT3 in human disease. *J. Clin. Immunol.* 35:615–623. https://doi.org/10.1007/s10875-015-0187-8

Warshauer, J.T., J.A. Belk, A.Y. Chan, J. Wang, A.R. Gupta, Q. Shi, N. Skartsis, Y. Peng, J.D. Phipps, D. Acenas, et al. 2021. A human mutation in STAT3 promotes type 1 diabetes through a defect in CD8+ T cell tolerance. *J. Exp. Med.* 218:e20210759. https://doi.org/10.1084/jem.20210759

Wickham, H. 2016. ggplot2: Elegant graphics for data analysis. Second edition. Springer-Verlag, New York, NY.

Wienke, J., W. Janssen, R. Scholman, H. Spits, M. van Gijn, M. Boes, J. van Montfrans, N. Moes, and S. de Roock. 2015. A novel human STAT3 mutation presents with autoimmunity involving Th17 hyperactivation. *Oncotarget.* 6:20037–20042.

Wohn, C., J.L. Ober-Blöbaum, S. Haak, S. Pantelyushin, C. Cheong, S.P. Zahner, S. Onderwater, M. Kant, H. Weighardt, B. Holzmann, et al. 2013. Langerin(neg) conventional dendritic cells produce IL-23 to drive psoriatic plaque formation in mice. *Proc. Natl. Acad. Sci. USA.* 110:10723–10728. https://doi.org/10.1073/pnas.1307569110

Wolk, K., S. Kunz, E. Witte, M. Friedrich, K. Asadullah, and R. Sabat. 2004. IL-22 increases the innate immunity of tissues. *Immunity.* 21:241–254. https://doi.org/10.1016/j.immuni.2004.07.007

Wolk, K., E. Witte, E. Wallace, W.D. Döcke, S. Kunz, K. Asadullah, H.D. Volk, W. Sterry, and R. Sabat. 2006. IL-22 regulates the expression of genes responsible for antimicrobial defense, cellular differentiation, and

mobility in keratinocytes: A potential role in psoriasis. *Eur. J. Immunol.* 36:1309–1323. https://doi.org/10.1002/eji.200535503

Woods, J., S.E. Pemberton, A.D. Largent, K. Chiang, D. Liggitt, M. Oukka, D.J. Rawlings, and S.W. Jackson. 2022. Cutting edge: Systemic autoimmunity in murine STAT3 gain-of-function syndrome is characterized by effector T cell expansion in the absence of overt regulatory T cell dysfunction. *J. Immunol.* 209:1033–1038. https://doi.org/10.4049/jimmunol.2100920

Yeste, A., I.D. Mascanfroni, M. Nadeau, E.J. Burns, A.M. Tukpah, A. Santiago, C. Wu, B. Patel, D. Kumar, and F.J. Quintana. 2014. IL-21 induces IL-22 production in CD4+ T cells. *Nat. Commun.* 5:3753. https://doi.org/10.1038/ncomms4753

Yu, H., D. Pardoll, and R. Jove. 2009. STATs in cancer inflammation and immunity: A leading role for STAT3. *Nat. Rev. Cancer*. 9:798–809. https://doi.org/10.1038/nrc2734

Zheng, Y., D.M. Danilenko, P. Valdez, I. Kasman, J. Eastham-Anderson, J. Wu, and W. Ouyang. 2007. Interleukin-22, a T(H)17 cytokine, mediates IL-23-induced dermal inflammation and acanthosis. *Nature*. 445:648–651. https://doi.org/10.1038/nature05505

Zhou, X., S.L. Bailey-Bucktrout, L.T. Jeker, C. Penaranda, M. Martínez-Llordella, M. Ashby, M. Nakayama, W. Rosenthal, and J.A. Bluestone. 2009. Instability of the transcription factor Foxp3 leads to the generation of pathogenic memory T cells in vivo. *Nat. Immunol.* 10:1000–1007. https://doi.org/10.1038/ni.1774

Supplemental material

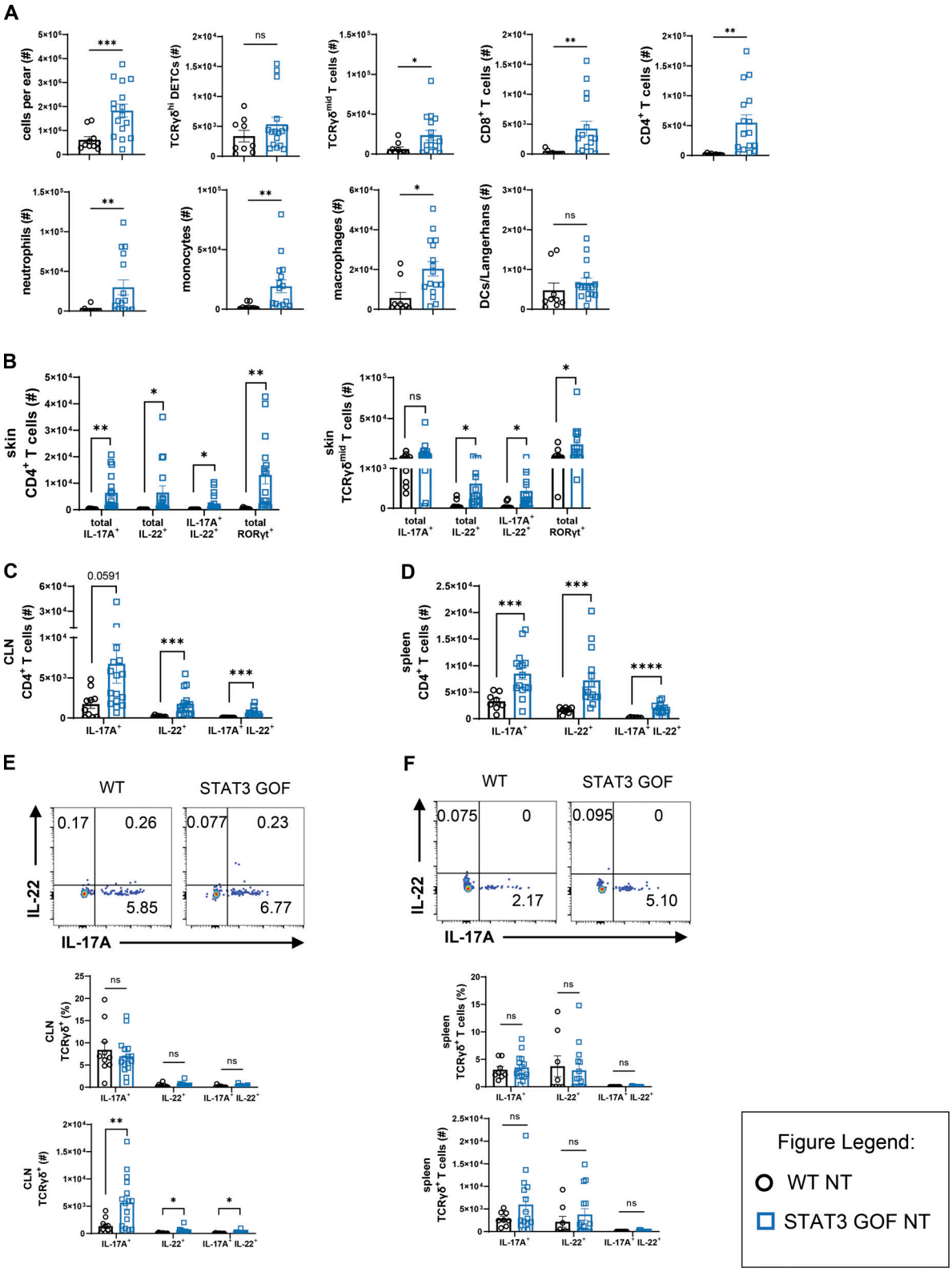

Figure S1. **Older adult STAT3 GOF (*Stat3*$^{p.G421R/+}$) mice develop spontaneous skin inflammation, related to** Fig. 1. **(A)** Absolute cell numbers of cells per ear and of skin immune cells of older adult WT and STAT3 GOF mice. **(B)** Absolute cell numbers of CD45.2$^+$ CD3$^+$ TCRγδ$^-$ CD8$^-$ CD4$^+$ (left) and CD45.2$^+$ CD3$^+$ TCRγδ^{mid} (right) T cells expressing RORγt, IL-17A, and/or IL-22 in the skin. **(C and D)** Absolute cell numbers of CD45.2$^+$ CD3$^+$ TCRγδ$^-$ CD8$^-$ CD4$^+$ T cells expressing IL-17A and/or IL-22 in the (C) CLN and (D) spleen. **(E and F)** Representative flow plots, quantification, and absolute cell number of IL-17A, and IL-22 expression in CD45.2$^+$ CD3$^+$ TCRγδ$^+$ T cells in the (E) CLN and (F) spleen. Cytokine expression assessed after PMA/ionomycin stimulation. Bars: mean ± SEM. Statistical significance determined by unpaired two-tailed or Welch's *t* test, *P < 0.05, **P < 0.01, ***P < 0.001, ****P < 0.0001. Data represent three experiments with 10–16 mice.

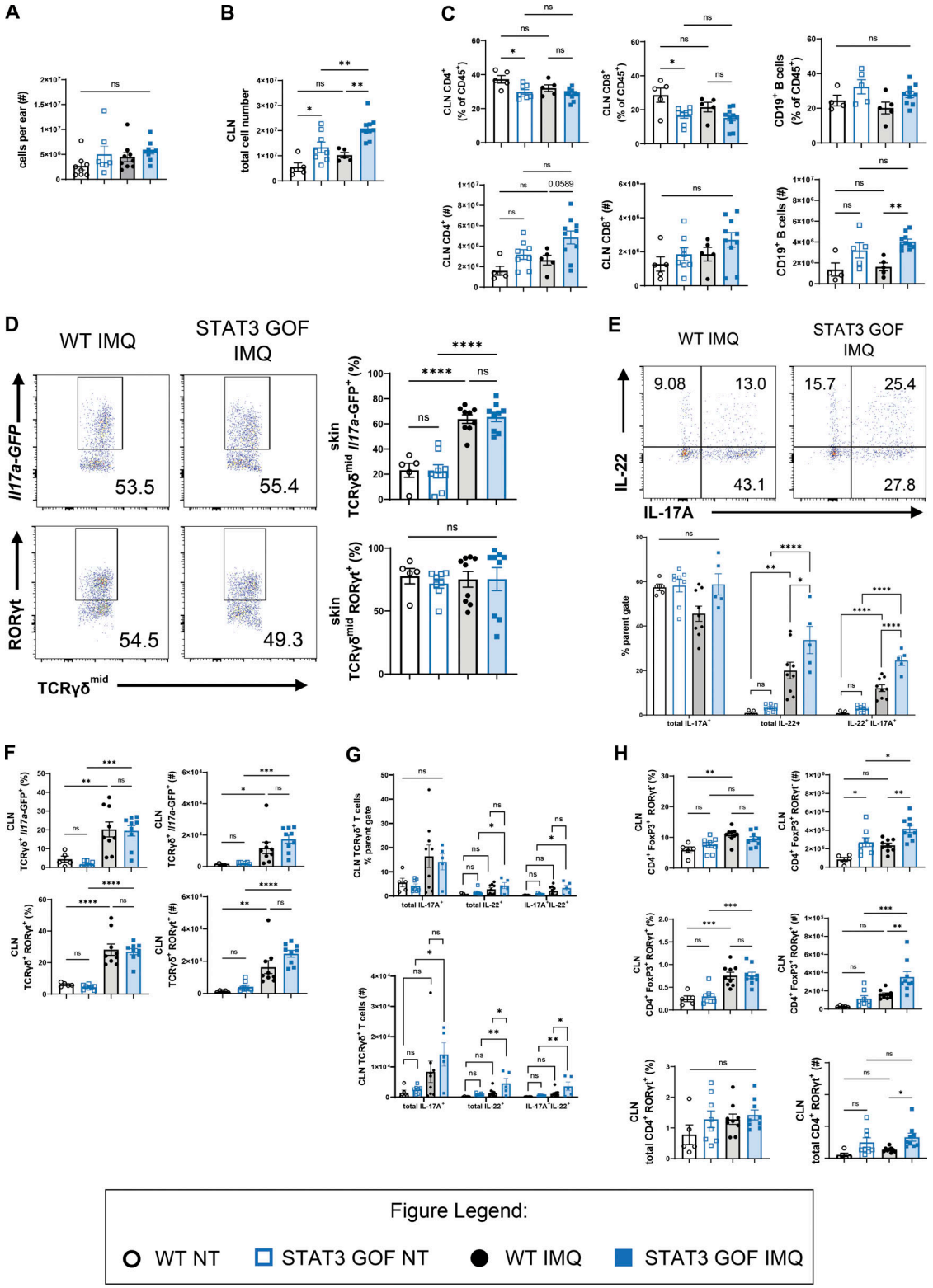

Figure S2. **Cell populations in skin and CLN of IMQ-treated young adult WT and STAT3 GOF mice, related to** Fig. 3**. (A)** Total number of cells per ear. **(B)** Total number of CLN cells. **(C)** Frequency and total number of lymphocyte populations in CLN. **(D)** Representative flow plots and frequency of CD45.2$^+$ CD3$^+$ TCRγδ^{mid} *Il17a*-GFP$^+$ and RORγt$^+$ cells. **(E)** Representative flow plots and frequency of CD45.2$^+$ CD3$^+$ TCRγδ^{mid} IL-17A$^+$ and IL-22$^+$ populations in skin. Cytokine expression assessed after PMA/ionomycin stimulation. **(F)** Frequency and number of CD45.2$^+$ CD3$^+$ TCRγδ$^+$ Il17a-GFP$^+$ or RORγt$^+$ populations in CLN. **(G)** Frequency and total number of CD45.2$^+$ CD3$^+$ TCRγδ^{mid} IL-17A$^+$ and IL-22$^+$ populations in skin. Cytokine expression assessed after PMA/ionomycin stimulation. **(H)** Frequency and total number of CD45.2$^+$ CD3$^+$ TCRγδ$^-$ CD4$^+$ FoxP3$^+$ RORγt$^-$, FoxP3$^+$ RORγt$^+$, and total RORγt$^+$ populations in CLN. Bars: mean ± SEM. Statistical significance was determined by one-way ANOVA with Sidak's multiple comparisons test. *P < 0.05, **P < 0.01, ***P < 0.001, ****P < 0.0001. Data represent three to four experiments with 5–12 mice.

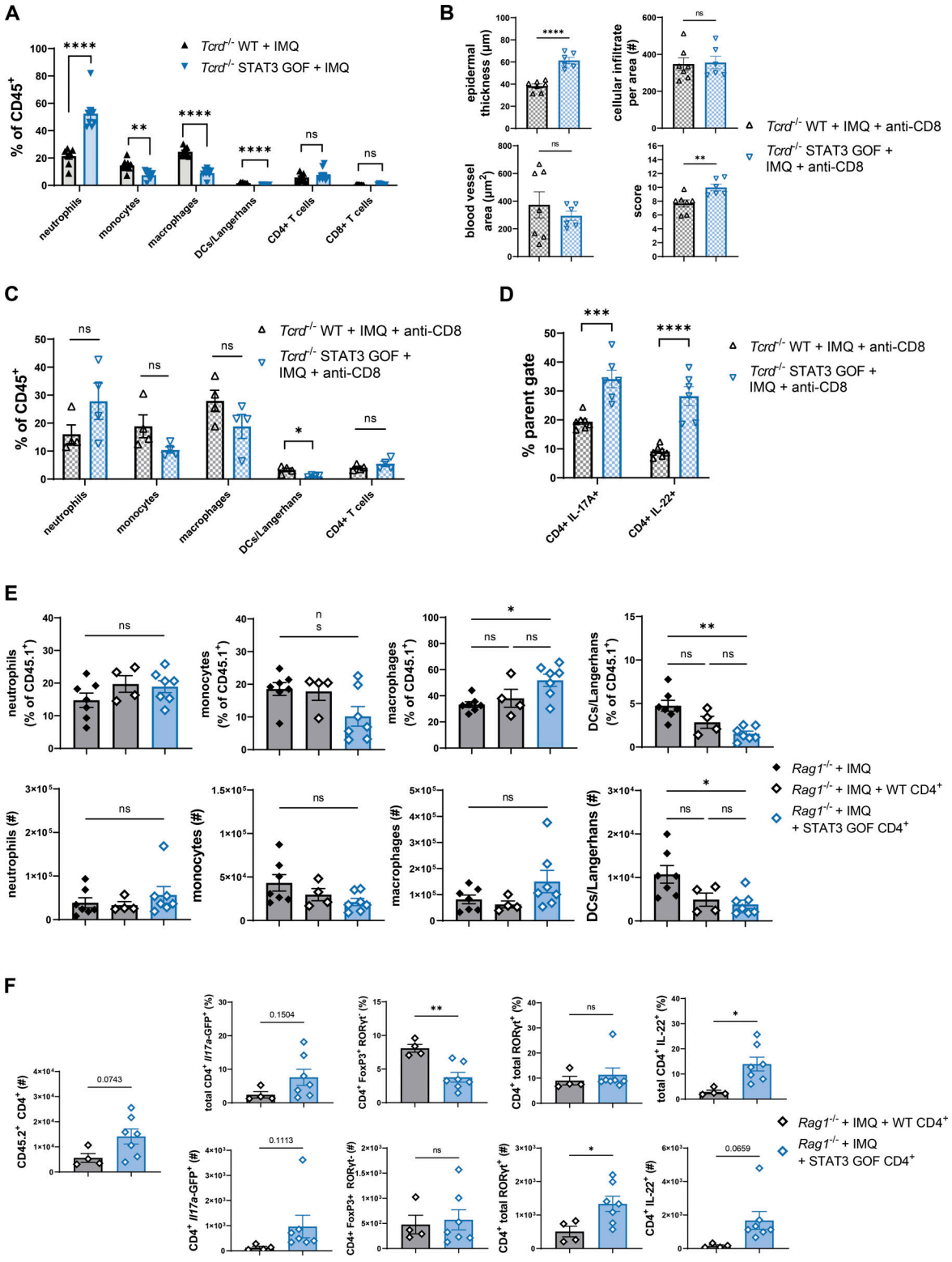

Figure S3. **CD4⁺ T cells are sufficient, and γδ T cells and CD8⁺ T cells are not required to mediate IMQ-induced inflammation in STAT3 GOF mice, related to** Fig. 4. **(A)** Skin immune cell frequencies of *Tcrd*$^{-/-}$ mice treated with IMQ. **(B)** Histological measurements from H&E sections of ear tissue of *Tcrd*$^{-/-}$ mice treated with IMQ + anti-CD8. **(C)** Skin immune cell frequencies of *Tcrd*$^{-/-}$ mice treated with IMQ + anti-CD8. **(D)** Frequency of CD45.2⁺ CD3⁺ TCRγδ⁻ CD8⁻ CD4⁺ T cells expressing IL-17A or IL-22 in *Tcrd*$^{-/-}$ mice treated with IMQ + anti-CD8. Cytokine expression assessed after PMA/ionomycin stimulation. **(E)** Quantification of skin immune cell frequencies of *Rag1*$^{-/-}$ control or adoptive transfer (CD4⁺ T cells) recipients treated with IMQ. **(F)** Quantification of total adoptively transferred CD45.2⁺ CD4⁺ T cells and transcription factor/cytokine frequencies of transferred CD4⁺ T cells found in skin. Bars: mean ± SEM. Statistical significance determined by unpaired two-tailed or Welch's *t* test (A–D and F) or one-way ANOVA with Sidak's multiple comparisons test (E). *P < 0.05, **P < 0.01, ***P < 0.001, ****P < 0.0001. Data represent three experiments with five to seven mice.

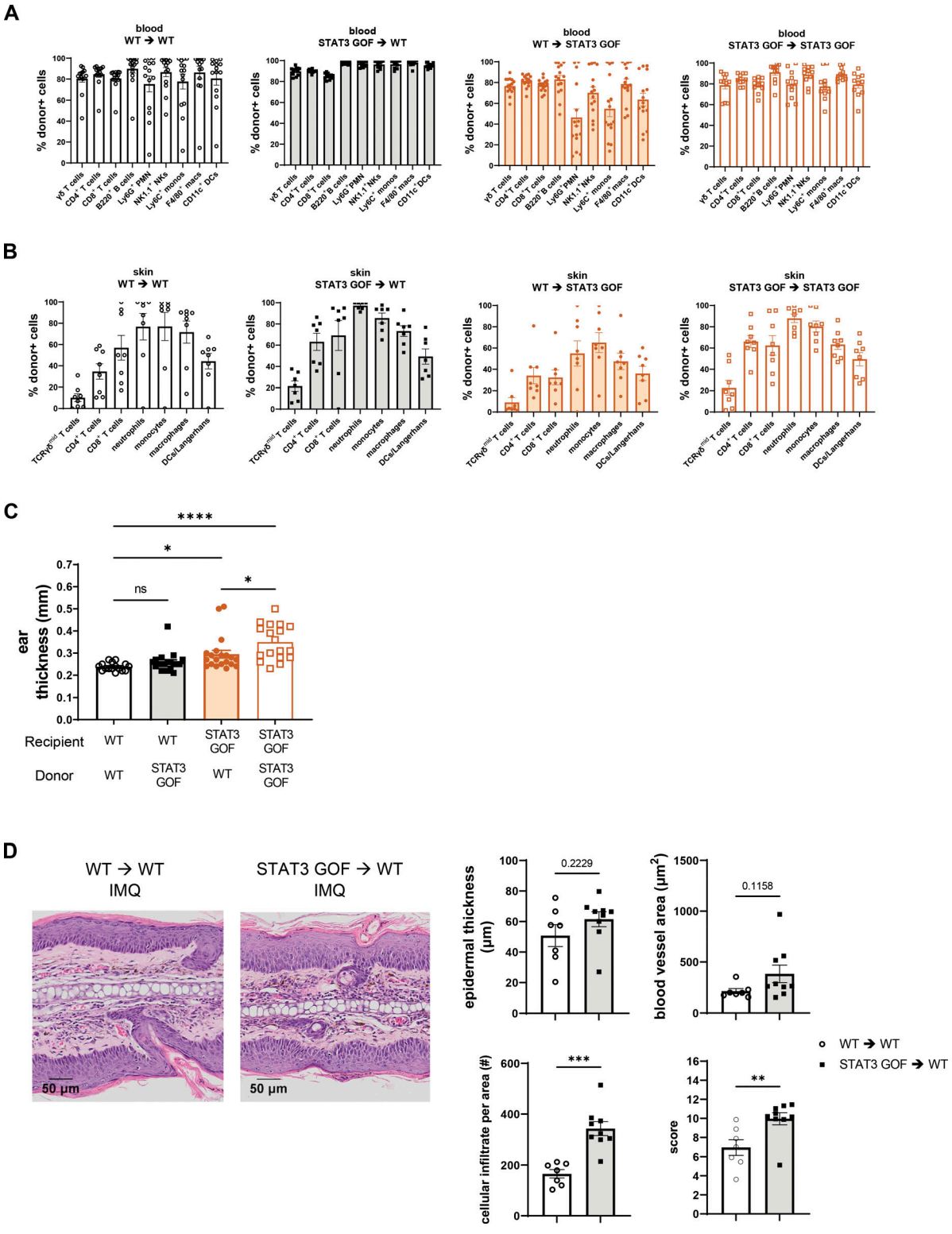

Figure S4. **STAT3 GOF BM can exacerbate inflammation in WT mice, related to Fig. 4. (A and B)** (A) Peripheral blood and (B) skin donor engraftment 12 wk after transplant in NT mice, including Ly6G+ polymorphonuclear neutrophils (PMNs). **(C)** Ear thickness of untreated BM chimeras 12 wk after transplant. **(D)** Histological measurements from H&E sections of ear tissue of IMQ-treated WT → WT or STAT3 GOF → WT chimeras. Bars: mean ± SEM. Statistical significance determined by one-way ANOVA with Sidak's multiple comparisons test (C) or unpaired two-tailed or Welch's *t* test (D). *P < 0.05, **P < 0.01, ***P < 0.001, ****P < 0.0001. Data represent four experiments with 8–12 mice per group.

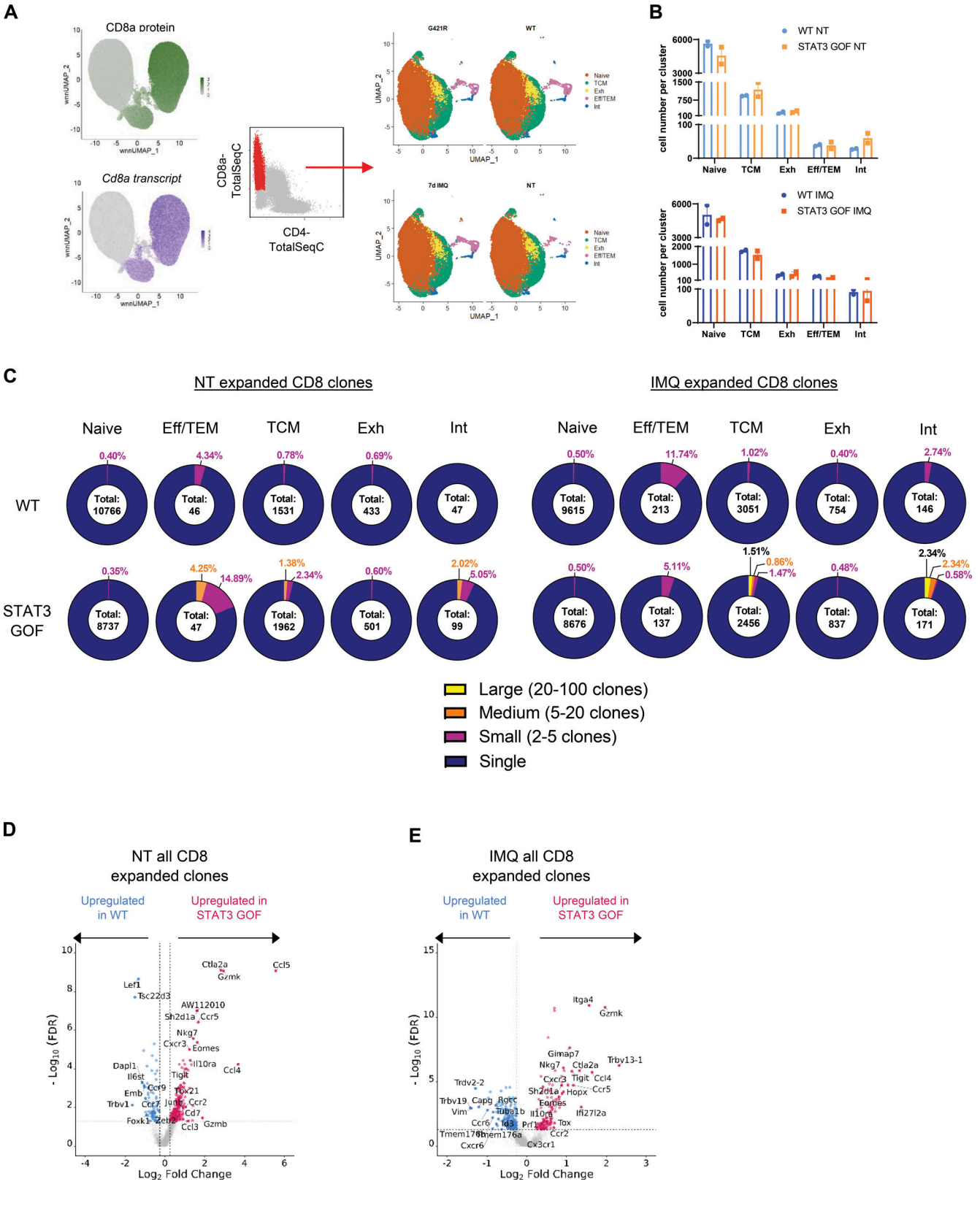

Figure S5. **STAT3 GOF T cell scRNA-seq after IMQ treatment, related to** Fig. 5. **(A)** Cellselector function was used to separate single-positive CD8 T cells, which were renormalized and reclustered based on CD44 and CD62L surface protein expression and canonical gene expression. **(B)** Frequencies of annotated CD8⁺ clusters based on genotype and treatment. **(C)** Clonotype frequency of the NT and IMQ-treated CD8⁺ T cells by annotated cluster generated with ScRepertoire. **(D and E)** Volcano plots showing differential expression (adjusted $P < 0.05$, average $\log_2$ fold change >0.25 or less than −0.25) in (D) NT CD8 expanded clones and (E) IMQ CD8 expanded clones, comparing WT and STAT3 GOF. Ribosomal genes, genes ending in -Rik, and genes beginning with Gm- are not labeled on volcano plots. Data are representative of one experiment with two mice/group.